Utrecht University

Institute for Theoretical Physics

Influence of Dzyaloshinskii-Moriya Interaction on Spin Waves and Magnon Spin Transport

Author:
Wiet van Lanschot

Supervisors:
Prof. Dr. Rembert Duine
Dr. Scott Bender
Drs. Camilo Ulloa

Master Thesis

June 2017

Abstract

Dzyaloshinskii-Moriya interaction (DMI) is an asymmetric exchange interaction that originates from spin-orbit couplings combined with a broken inversion symmetry. Motivated by recent experimental developments, we investigate the effects of DMI strength on spin waves in a 2D lattice spin model with easy-axis anisotropy and an external magnetic field. Furthermore, we consider a setup that consists of a ferromagnetic medium bounded by two metallic reservoirs. We compute the transverse and longitudinal spin current in this setup using the stochastic Landau-Lifshitz-Gilbert equation with appropriate boundary conditions. We find that the transverse spin current vanishes, whereas the longitudinal spin current is influenced by DMI.

Contents

Preface . . . 3

1 Short Introduction to Spin Waves **8**

1.1 Spin waves explained using a 1D lattice model . . . 8

1.2 The Landau-Lifshitz-Gilbert Equation . . . 11

1.3 DMI . . . 11

2 Influence of DMI on Spin Waves **13**

2.1 Equilibria coinciding with an external magnetic field . . . 14

2.1.1 Linearzing around an axial equilibrium . . . 15

2.1.2 Linearzing around a planar equilibrium . . . 16

2.2 Expanding the Landau-Lifshitz equation . . . 17

2.2.1 Linearzing around an axial equilibrium . . . 19

2.2.2 Linearzing around a planar equilibrium . . . 21

2.3 Linearizing around equilibria not coinciding with the external magnetic field . . . 23

2.3.1 Linearizing around an equilibrium not coinciding with the magnetic field in the axial regime . . . 23

2.3.2 Linearizing around an equilibrium not coinciding with the magnetic field in the planar regime . . . 28

2.4 Consequences for our setup . . . 31

3 Influence of DMI on Magnon Spin Currents **33**

3.1 A solution for ψ at the interface . . . 35

3.2 The transverse interfacial spin current 36
3.3 A solution for ψ in the bulk 38
3.4 The transverse bulk spin current 39
3.5 The longitudinal spin current evaluated at $x = d$ 41

4 Conclusion and Outlook **43**

Acknowledgements **45**

Bibliography **46**

Appendices **49**

A Calculation of the equation of motion **49**

B Calculation of the boundary conditions **51**

C Computation of the interfacial transverse current **54**

D Computation of ψ_B **58**

E Computation of the transverse bulk current **62**

F Dimensional analysis of the currents **75**
F.1 Interfacial current 75
F.2 Bulk current 76

G Computation of the longitudinal current with DMI at $x = d$ **77**
G.1 The interfacial longitudinal current at $x = d$ 77
G.2 The bulk longitudinal current at $x = d$ 79
G.3 Adding the currents 80

Preface

Spintronics (short for spin transport or spin based electronics) aims to understand and control the behaviour of electrons with an emphasis on their spin degrees of freedom, rather than only on their charge. It is a relatively young field of study, where its conception is generally considered to be the discovery of the giant magnetoresistive effect in 1988, a discovery that in 2007 was awarded with the Nobel Prize[1, 2]. The Nobel committee argued that

> *"Applications of this phenomenon have revolutionized techniques for retrieving data from hard disks. The discovery also plays a major role in various magnetic sensors as well as for the development of a new generation of electronics. The use of Giant Magnetoresistance can be regarded as one of the first major applications of nanotechnology."*[3]

Conventional electronics describes the behaviour of electric excitations that exist in conducting, semiconducting and insulating materials. An electric current has massive particles (electrons) moving through a medium. Spintronics deals with spin currents, one example of which arises in the context of magnetic excitations that exist in magnetic materials. In a ferromagnetic medium, for example, all particles share the same spin. If one particle has an excitation that leads to the direction of its spin to deviate from its equilibrium direction, this excitation will, through various mechanisms, lead to the excitation traveling through the medium, like a wave. Quantizing this wave, we can regard it as a quasiparticle travling through the medium. This quasiparticle is known as the magnon. For magnon transport, there is no movement of massive particles, only excitations of the magnetic field of particles. A short, but more thorough introduction on spin waves is given in chapter 1.

In the future, we may be able to manipulate the spin degrees of freedom in such a way that we can use them to transmit information. This is the reason that spintronics is such a promising field of study with regard to its possible applications. As spin waves do not involve the motion of electrons, they are free of Joule heat dissipation[5], which can lead to a decrease in energy consumption of information transmitting systems. Furthermore, the use of spin waves for the transmission of information allows operations with vector rather than scalar variables[5]. This could have many advantages such as increased data processing speed as well as an even larger decrease in electric power consumption[1].

With so many potential applications, it is not surprising that fundamental research into spintronics has grown recently, with many exciting developments having occurred in the past few years[6]. The spin Hall effect is an example of a recent discovery that has rapidly grown into its own subfield[7]. Due to different phenomena, for example the presence of spin-orbit interactions, it is possible to generate a spin current transverse to the direction of an electric current through a (semi)conducting lateral surface. This is further clarified in Fig. 1. The phenomenon also leads to the inverse spin Hall effect:

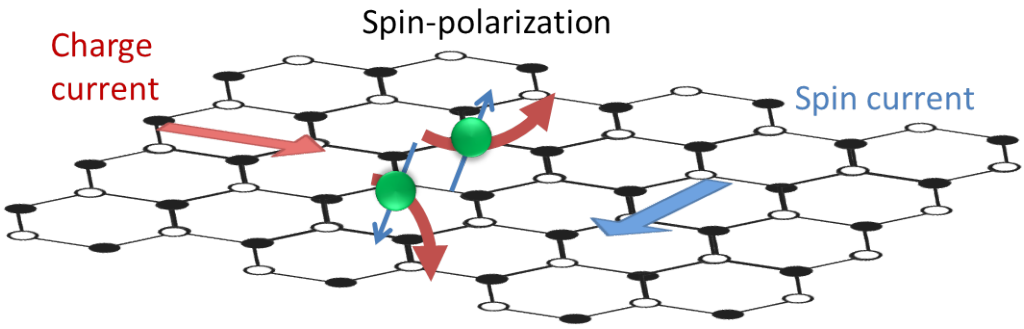

Figure 1 – If a charge current is applied to a (semi)conducting lateral surface, the spin Hall effect will lead to the appearance of a spin current transverse to the direction of the charge current. Figure taken from [9].

if a spin current is injected into a (semi)conducting lateral surface, a charge current transverse to the spin current will appear. Research into this effect has enabled us to use the spin Hall effect as a tool to detect, measure and generate[8] spin currents. We should note that, in this case, the spin current still involves the motion of electrons and not magnons, with the direction in which the electrons move depending on their spin. This is why this type of spin current is also know as an electron spin current.

We now regard a setup in which an (electron) spin current is generated by injecting an electric current into the sample, and have this sample share an interface with a second, insulating, magnetic sample. As the second sample is an insulator, the electric current in the first, conducting sample will not be transmitted into the second sample. The same goes for the electron spin current. It has been shown, however, that the electron spin current in the (semi)conducting sample will induce a *magnon* spin current in the insulating sample[12]. This way, we can (indirectly) electrically induce a magnon spin current in an insulating, magnetic sample.

The generation of a magnon spin current in an insulating sample through the spin Hall effect has been experimentally verified using the following setup: we view an insulating magnetic sample, connected to (semi)conducting metallic lateral surfaces at both ends. A current is applied to one of the conducting metals, leading to an electron spin current transverse to this electric current due to the spin Hall effect. The spin current will also propagate through the insulating sample as a magnon spin current, leading to another electron spin current in the other (semi)conducting sample. This will, in turn, lead to an electric current in the other (semi)conducting sample through the inverse spin Hall effect, which can be measured. The setup is illustrated in Fig. 2.

Another means of magnon spin current generation in magnetic, insulating materials is through thermal gradients, following the discovery of the spin Seebeck effect. This effect seems to originate, amongst others, in the interaction between magnons and phonons[10]. In the spin Seebeck effect, a temperature gradient applied to a magnetic, insulating sample will lead to a spin current through this sample (see Fig. 3)[14]. This effect has been

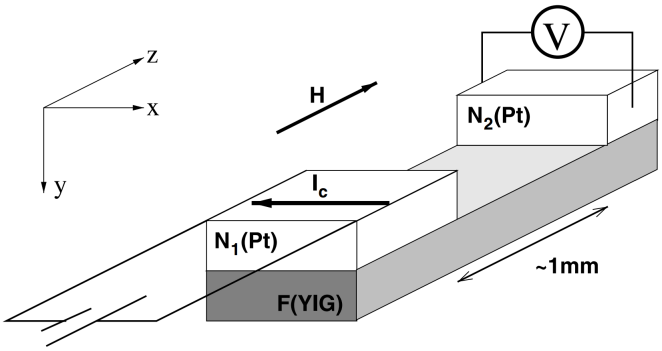

Figure 2 – Experimental setup to confirm electrically driven magnon spin currents. An electric current in one conducting sample will lead to a spin current transverse to the electric current due to the spin Hall effect, which will propagate through the insulating material, denoted by F(YIG) in the figure. This spin current will lead to an electric current transverse to this spin current in the second conducting sample due to the inverse spin Hall effect. Figure taken from [16].

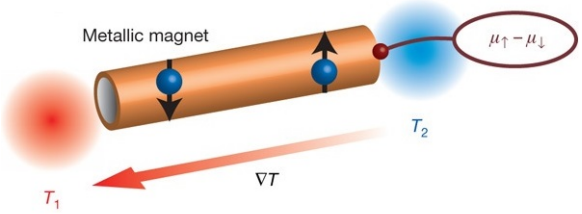

Figure 3 – A temperature gradient applied to a magnetic sample leads to a spin current through this sample. Figure based on figure taken from [10].

experimentally verified. The measurement of this effect relies on the inverse spin Hall effect[10]: at the ends of an insulating magnetic medium, two (semi)conducting samples are placed. Upon generating a magnon spin current in the insulating medium through the application of a thermal gradient, this spin current will also propagate through the (semi)conducting samples as an electron spin current. Inside these conducting metals, a charge current transverse to the spin current will appear due to the inverse spin Hall effect. Measuring this charge current leads to the conclusion that a spin current has appeared in the insulating sample. This setup is shown in Fig. 4.

Another interesting new phenomenon is the magnon Hall effect, which is analogous to the Hall effect. The Hall effect was discovered by Hall in 1879[11]: if we apply a magnetic field perpendicular to the direction of an electric current, an additional electric current will appear, perpendicular to both the original electric current and the magnetic field. This phenomenon is driven by the Lorentz force. In the magnon Hall effect, analogously, we view a magnon spin current and apply a magnetic field, which leads to the appearance of a magnon spin current transverse to the original spin current. Rather than by Lorentz force, the magnon Hall effect is theorized to be driven by the Dzyaloshinskii-Moriya

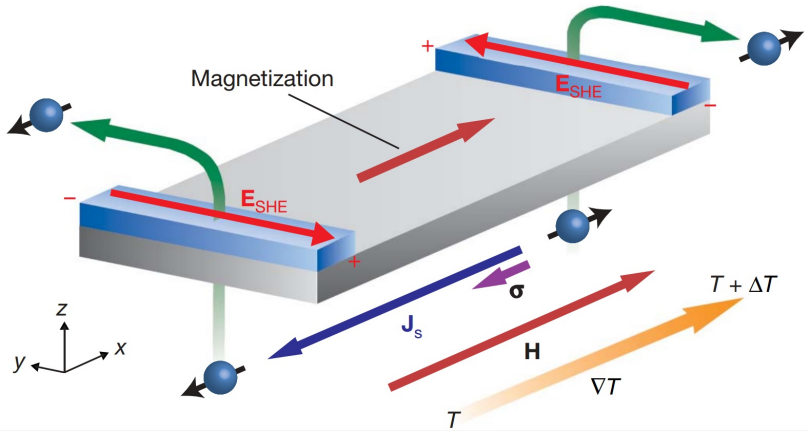

Figure 4 – Experimental setup to measure the Seebeck effect. A thermally generated spin current in an insulating sample leads to electric currents transverse to the spin current in conducting metals at the ends of the insulating sample through the inverse spin Hall effect. Figure taken from [10].

interaction (DMI)[13]. One way of generating the (longitudinal) spin current is through the spin Seebeck effect, by use of a temperature gradient. For a current generated this way, the magnon Hall effect has been experimentally observed[13]. This experiment is further clarified in Fig. 5.

It has been theorized that an electrically induced spin current will also exhibit the magnon Hall effect[17]. This electrically induced magnon Hall effect is illustrated in Fig. 6. In this thesis, we set out to study the electrically induced magnon Hall effect by computing the transverse current under the influence of an external magnetic field and DMI. In the first chapter, some background on spin waves and DMI will be given. In the second chapter, we look at the influence of different interactions on the free energy of spin waves. We will use a 2D lattice model of a ferromagnet with easy-axis anisotropy to examine 4 interactions, and see how different ratios between these interactions affect the free energy, dispersion relations, the direction of the equilibrium of individual spins and the ground states. We will see that the ratios of the different interaction strengths have a very significant effect on the spin waves.

Using this knowledge, we define a setup in which we can perform our calculations in the third chapter. We will look at the influence of DMI on transverse and longitudinal spin currents through a ferromagnet bounded by metallic reservoirs. We will see that, even with DMI present, the transverse current vanishes. We will also see that DMI does have an effect on the longitudinal current. We will finally discuss the merits and drawbacks of this model.

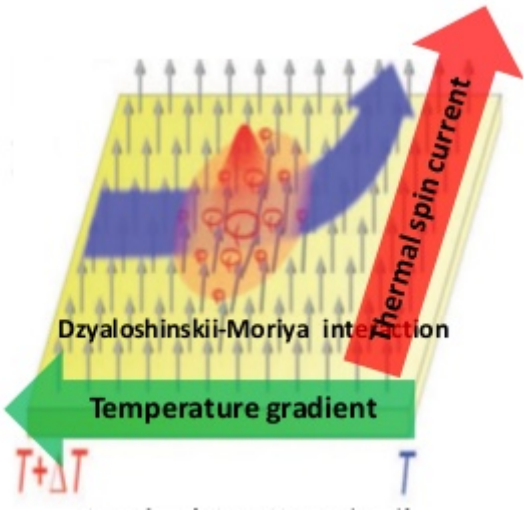

Figure 5 – The magnon Hall effect with a spin current generated by a temperature gradient. The blue arrow represents a spin current being bent into the transverse direction. The grey arrows represents the external magnetic field. Figure taken from [15].

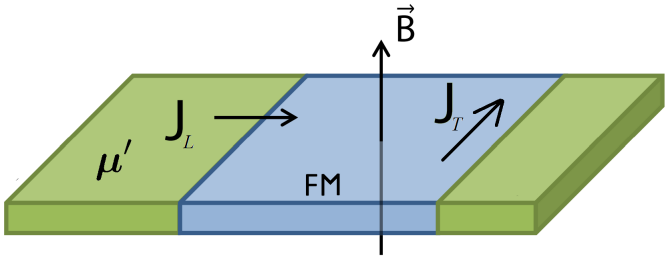

Figure 6 – The magnon Hall effect generated by a magnon potential gradient. We see a spin accumulation μ' on one side, and a resulting longitudinal spin current J_L. If the magnon Hall effect also applies to electrically induced magnon spin currents, we expect to see a transverse magnon spin current to appear. Figure based on figure taken from [18].

Chapter 1

Short Introduction to Spin Waves

The spin of an electron, or its intrinsic magnetic moment, can only be understood through quantum mechanics. To form an intuitive understanding of spin waves, however, we can use a classical model in which each spin is represented by a small magnet. We will first give a simple example of a spin wave by looking at a 1D lattice of spins with two kinds of interactions. We will then examine the Landau-Lifshitz-Gilbert equation, an equation that describes the precessional motion of the magnetization of a material. Finally, we will take a closer look at DMI.

1.1 Spin waves explained using a 1D lattice model

We take a 1D lattice model (see Fig. 1.1) and assume that each electron interacts with its environment in two different ways: by the Heisenberg exchange interaction and by the interaction of the spins with an external magnetic field. The Heisenberg exchange interaction describes the energy cost of the relative orientation between two neighbouring spins:

$$H_{XC} = -\frac{J}{2}\mathbf{S}_1 \cdot \mathbf{S}_2.$$

Here, $\mathbf{S}_1$ and $\mathbf{S}_2$ represent unit vectors that point in the direction of the magnetic field generated by the small magnets that represent the spins, and J represents the exchange constant of the material. The value of J depends on the material. For $J > 0$, the material is called ferromagnetic, and the spins will favour parallel alignment. For $J < 0$, the material is called antiferromagnetic, and the spins will favour antiparallel alignment. In this thesis, we are only concerned with ferromagnetic materials.

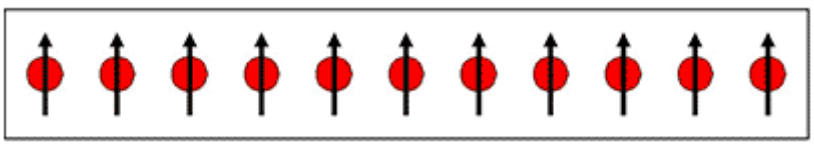

Figure 1.1 – A 1D ferromagnetic lattice of spins, all aligned with eachother. Picture taken from [23].

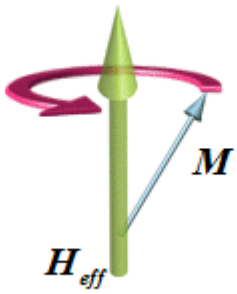

(a) A spin precessing around its equilibrium. Figure taken from [24].

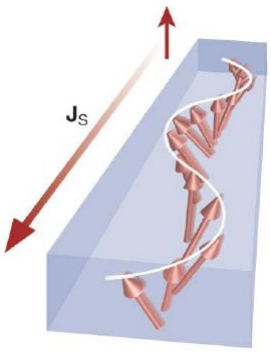

(b) A spin wave. The wave travels in the direction of J_s, with a magnetic field pointing upwards. Figure taken from [22].

Figure 1.2 – Precession of a spin around its equilibrium can cause a wave propagating through the medium.

The interaction of the spins with an external magnetic field describes the energy cost of the orientation of a single spin with respect to an external magnetic field $\mathbf{B}$:

$$H_B = -\mathbf{B} \cdot \mathbf{S}.$$

We see that this interaction will favour an alignment of each spin with an external magnetic field. If we were to pull one spin from its equilibrium position, we can imagine the spin starting to precess around its equilibrium position. This precessing motion is shown in Fig. 1.2a.

Over time, its deviation from the equilibrium position will get smaller and smaller due to a process called damping, analogous to a swinging pendulum that will decrease its deviation of its equilibrium position over time. An illustration of this damping is shown in Fig. 1.3.

In our 1D ferromagnetic lattice of spins, all the spins will align with the magnetic field when at rest. If we now were to push the left spin, so that it will start to precess around its equilibrium position, this spin will interact with its neighbor due to the Heisenberg exchange interaction. This will cause its neighbor to start precessing around its equilibrium as well. This in turn, will give the next neighboring spin a push as well, and so on, leading to a wave propagating through the lattice. This is an example of a very simple spin wave. In Fig. 1.2b an illustration of a spin wave is given.

We can quantize the spin wave and associate a quasiparticle with it: the magnon. If we were to examine a ferromagnetic medium with an external magnetic field at zero

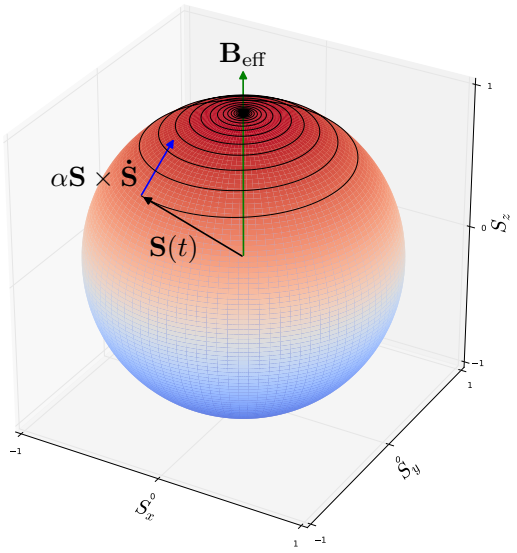

Figure 1.3 – A representation of spin precession with damping. The direction of $\mathbf{B}_{eff}$ is what we refer to as our equilibrium direction. The Gilbert damping term is shown pointing toward the equilibrium, with the blue arrow. Due to the damping process, the precession of a spin around its equilibrium prosition will die out over time. Picture taken from [26].

temperature, we would see all spins aligning with this field and staying there. We can now imagine increasing the energy in the system, which we can do by adding electric energy, increasing the temperature, and many other ways. Adding energy to the system will lead to excitations of individual spins. These excitations will then propagate through the lattice. We could also view this system in a quantummechanical way, by viewing the lattice of spins as still being at complete rest, and having more magnons appearing and propagating through the medium as the temperature increases.

1.2 The Landau-Lifshitz-Gilbert Equation

The Landau-Lifshitz-Gilbert Equation (LLG) is a differential equation that describes the magnetization $\mathbf{m}$ of a material. It is an extension of the Landau-Lifshitz equation. In the Landau-Lifshitz equation, $\mathbf{m}$ is a continuous quantity, as opposed to the discrete $\mathbf{S}$, that denotes individual spins:

$$\hbar\partial_t\mathbf{m} = -\gamma\mathbf{m} \times \frac{\delta E}{\delta \mathbf{m}}, \tag{1.1}$$

where γ is the gyromagnetic ratio (from here on assumed 1) and E is the total energy of the system, which arises from a combination of the external magnetic field as well as other possible contributions. Here, $\frac{\delta E}{\delta \mathbf{m}}$ can also be written as the effective field $\mathbf{H}_{eff}$. This equation tells us how the precession of the magnetization will dynamically evolve. The precession, as described in the equation above, will continue indefinitely. In practice, the precession will damp over time, causing the spin to re-align with its equilibrium position, as explained before. Gilbert extended the Landau-Lifshitz equation to include this damping:

$$\hbar\partial_t\mathbf{m} = -\mathbf{m} \times \mathbf{H}_{eff} - \alpha_G\mathbf{m} \times \hbar\partial_t\mathbf{m}, \tag{1.2}$$

where α_G (which is greater than zero) is the Gilbert damping parameter. The damping itself is a consequence of the magnetization interacting with other degrees of freedom in the material. Ultimately, the damping of the spin precession will thus lead to heating of the material.

1.3 DMI

The Dzyaloshinskii-Moriya Interaction (DMI) is a consequence of spin-orbit interactions combined with a broken inversion symmetry[27]. The interaction acts in a plane. If we let this plane be normal to $\hat{z}$, DMI can be written as

$$H_{DMI} = \frac{D}{2}[\hat{x} \cdot (\mathbf{m} \times \partial_y\mathbf{m}) - \hat{y} \cdot (\mathbf{m} \times \partial_x\mathbf{m})],$$

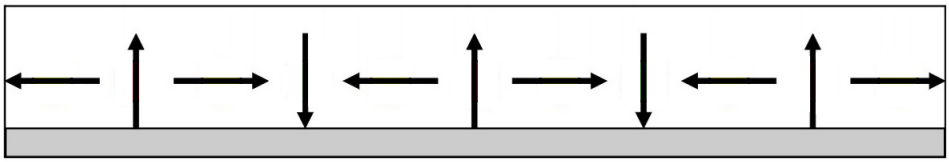

Figure 1.4 – DMI causes neighbouring spins to favour orthogonal orientation. Image taken from [28].

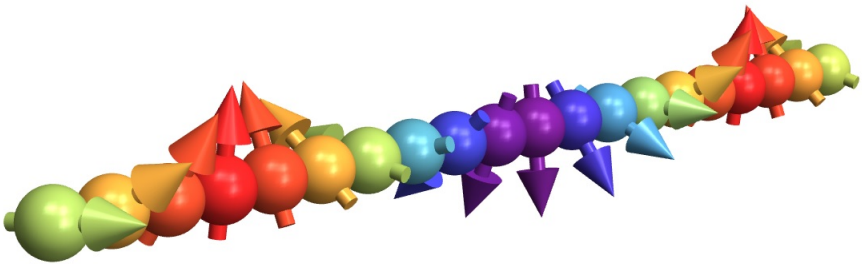

Figure 1.5 – Under the right conditions, DMI causes the ground state of a system to become unstable and form a spiral. The colors indicate different angles.

where D is the DMI constant. Due to the cross product, two neighboring spins will favour an orthogonal orientation in the plane in which the DMI is present, as is shown in Fig. 1.4. We can imagine DMI competing with Heisenberg exchange interaction, which could lead to a spiraling structure of the spins, as shown in Fig. 1.5. A system in which this spiraling structure was the ground state of a spin wave has been observed[32].

As DMI depends on a broken inversion symmetry, it vanishes in inversion-symmetric structures and can therefore be excluded for most simple bulk materials. Much more relevant for DMI are surface or interface geometries, in which the inversion symmetry is broken[27], as well as crystals with unconventional geometries, in particular multilayer crystals, such as pyrochlore structures.

Chapter 2

Influence of DMI on Spin Waves

We will investigate the dispersion relations of spin waves traveling through a ferromagnetic medium, and in particular the influence of DMI. In our setup, we will consider four different kinds of interaction: Heisenberg exchange interaction, interaction of spins with a magnetic field, DMI and anisotropy.

Of these four interactions, three have been covered in chapter 1. The fourth, anisotropy, concerns anisotropic properties of the material. It originates from spin orbit couplings and dipole-dipole interactions. It means that, for a single spin, an orientation parallel to a certain axis is favored:

$$H_{ANI,x} = -\frac{K_x}{2} m_x^2.$$

In this formula, spins favor parallel alignment with the x-axis, which is why this kind of anisotropy is also referred to as *easy axis*-anisotropy. As can be seen from the formula, it doesn't matter whether the spin is pointed in the $+x$- or $-x$-direction.

We consider spins arranged in a 2D square lattice, where we choose the axes in such a way that the lattice lies in the (x, y)-plane. An illustration of this setup is shown in Fig. 2.1. We will investigate how different ratios of the interaction strengths will affect the setup, and the consequences for the calculation of the transverse current that we

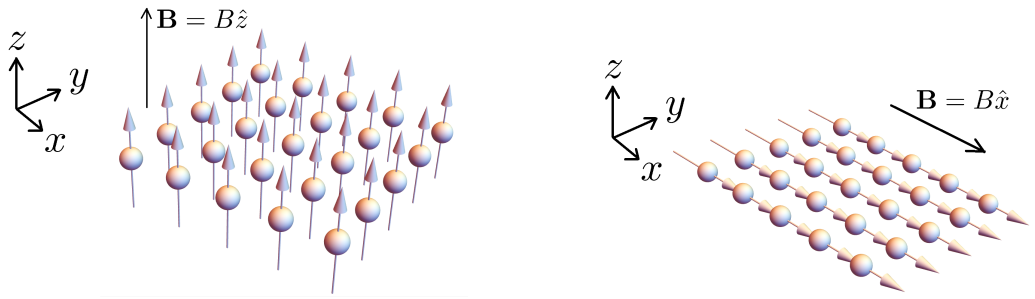

(a) The lattice in the z-regime. **(b)** The lattice in the x-regime.

Figure 2.1 – A 2D lattice of spins with their equilibrium positions aligned with the magnetic field **B**.

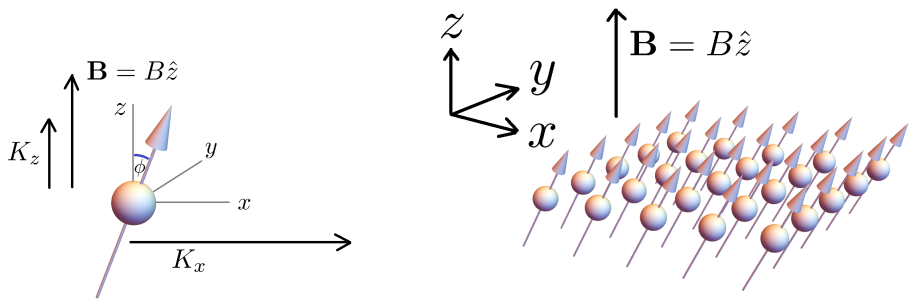

(a) The equilibrium position of a single spin being "pulled" away from the direction of the magnetic field.

(b) A lattice with spins in an equilibrium position that isn't aligned with the magnetic field. Note that all spins could also make an angle of $-\phi$ and be in equilibrium.

Figure 2.2 – If an anisotropy perpendicular to the external magnetic field (K_x in this example) is sufficiently large enough, the equilibrium position of a spin will make a nonzero angle ϕ with the direction of the external magnetic field. We will see that a nonzero ϕ appears if $K_x > B + K_z$.

will perform in the next chapter. When the influence of DMI is large when compared to other interactions, the ground state becomes unstable, and takes on a spiraling form, as illustrated in Fig. 1.5. In our later calculations, we would like a setup where this unstable ground state does not appear.

Also, the effects of anisotropy, especially in directions perpendicular to the applied external magnetic field, should be considered. Intuitively, we understand that the anisotropy will have a certain influence on the equilibrium position of the spins. For some anisotropy strenghts, the equilibrium position of the spins will not be parallel to the external magnetic field, which can drastically complicate calculations. An illustration of the equilibrium position of spins not aligned with the external magnetic field is shown in Fig. 2.2. We need to find out how big this influence is, and choose our magnetic field strength accordingly when we move towards calculating the transverse spin current. In our final setup, we will use an external magnetic field with an interaction magnitude far greater than that of the anisotropies and DMI.

2.1 Equilibria coinciding with an external magnetic field

As stated before, we consider a 2D square lattice with a lattice constant a, where we choose the axes in such a way that the lattice lies in the (x, y)-plane. The system will have an energy of

$$E_{TOT} = \int dx H_{TOT} = \int dx (H_{XC} + H_{DMI} + H_B + H_{ANI}),$$

where

$$\begin{aligned} H_{XC} &= -\frac{J_{xc}}{2}\mathbf{m}\cdot\nabla^2\mathbf{m}, \\ H_{DMI} &= \frac{D}{2}\left[\hat{x}\cdot(\mathbf{m}\times\partial_y\mathbf{m}) - \hat{y}\cdot(\mathbf{m}\times\partial_x\mathbf{m})\right], \\ H_B &= -\mathbf{B}\cdot\mathbf{m}, \\ H_{ANI} &= -\frac{K_z}{2}m_z^2 - \frac{K_x}{2}m_x^2. \end{aligned}$$

Here, H_{XC} denotes the Heisenberg exchange interacion, H_{DMI} the Dzyaloshinskii-Moriya interaction, H_B the interaction the spins with the magnetic field $\mathbf{B}$ and H_{ANI} the easy-axis anisotropies in the z- and x-direction. A straightforward calculation leads to

$$\begin{aligned} \frac{\delta E}{\delta m_x} &= -J\nabla^2 m_x + D\partial_x m_z - B_x - K_x m_x, \\ \frac{\delta E}{\delta m_y} &= -J\nabla^2 m_y + D\partial_y m_z - B_y, \\ \frac{\delta E}{\delta m_z} &= -J\nabla^2 m_z - D(\partial_x m_x + \partial_y m_y) - B_z - K_z m_z. \end{aligned} \tag{2.1}$$

We will derive the equations of motion by linearizing around the equilibrium, using the Landau-Lifschitz equation (Eq. 1.1). Throughout this chapter we will view the system in two separate regimes. We define the axial regime and the planar regime to have a magnetic field $\mathbf{B}$ pointed along the z-axis and the x-axis, respectively. These different regimes are illustrated in Fig. 2.1.

2.1.1 Linearzing around an axial equilibrium

We assume $\mathbf{B} = B\hat{z}$ and $K_x = 0$, so that the equilibrium position of the spins is in the z-direction. We now consider small deviations from the equilibrium in the in the x- and y-direction, writing them as δm_x and δm_y, respectively. We consider these deviations so small that we can neglect δm_x^2 and δm_y^2, which leads to the z-component having a length of $\sqrt{1-\delta m_x^2-\delta m_y^2} = 1$. We can thus take $\mathbf{m} = (\delta m_x, \delta m_y, 1)^T$. Using equation 1.1, we find

$$\begin{aligned} \hbar\partial_t(\delta m_x) &= (B+K_z)\delta m_y - J\nabla^2\delta m_y, \\ \hbar\partial_t(\delta m_y) &= J\nabla^2\delta m_x - (B+K_z)\delta m_x. \end{aligned}$$

Taking Ansatzes $\delta m_x = A_x e^{i(\mathbf{k}\cdot\mathbf{x}-\omega t)}$ and $\delta m_y = A_y e^{i(\mathbf{k}\cdot\mathbf{x}-\omega t)}$ we see

$$\begin{aligned} -i\hbar\omega A_x &= (B+K_z+J|\mathbf{k}|^2)A_y, \\ -i\hbar\omega A_y &= -(B+K_z+J|\mathbf{k}|^2)A_x, \end{aligned}$$

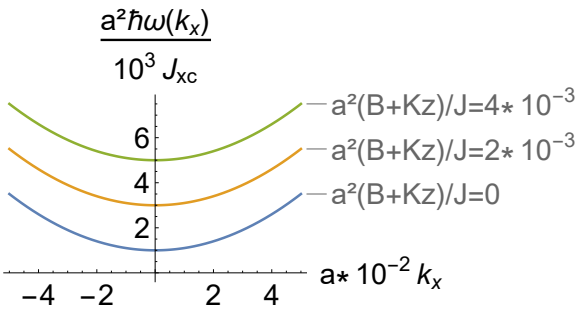

Figure 2.3 – The (ω, k_x) dispersion relation, plotted for different values of $B + K_z$. An increase in B has the same effect as an increase in K_z. An increase in B and K_z lead to a larger 'gap' between the minimum and zero. Due to rotational symmetry, the (ω, k_y) dispersion relation look the same.

which leads to

$$\begin{pmatrix} i\hbar\omega & (B + K_z + J|\mathbf{k}|^2) \\ -(B + K_z + J|\mathbf{k}|^2) & i\hbar\omega \end{pmatrix} \begin{pmatrix} A_x \\ A_y \end{pmatrix} = \begin{pmatrix} 0 \\ 0 \end{pmatrix},$$

which gives us the dispersion relation

$$\hbar\omega = J|\mathbf{k}|^2 + B + K_z. \tag{2.2}$$

This dispersion relation is plotted for multiple values of B and K_z in Fig. 2.3. We see that, for increasing B and K_z, a 'gap' appears. Physically, this means that the lowest excited state has a greater energy and frequency than without the 'gap'. It is therefore impossible to find particles with an energy level between the vacuum state and the first excited state. A greater amount of energy is thus needed to have a particle 'jump' to its lowest excited state. In a system of spins at zero temperature with a large external magnetic field, adding a small amount of energy, like a small increase in temperature or a moving electron (i.e. a small injected electric current), will therefore not lead to any excitations in the system, as the 'gap' will not be overcome by these small energy increases.

2.1.2 Linearzing around a planar equilibrium

We assume $\mathbf{B} = B\hat{x}$ and $K_z = 0$, so that the equilibrium position of the spins is in the x-direction. Considering fluctuations around this equilibrium in the y- and z-direction, we can take $\mathbf{m} = (1, \delta m_y, \delta m_z)^T$. Using equation 1.1, we find

$$\begin{aligned} \hbar\partial_t(\delta m_y) &= J\nabla^2\delta m_z - (B + K_x)\delta m_z - D\partial_y(\delta m_y), \\ \hbar\partial_t(\delta m_z) &= -J\nabla^2\delta m_y + (B + K_x)\delta m_y + D\partial_y(\delta m_z). \end{aligned}$$

Taking Ansatzes $\delta m_y = A_y e^{i(\mathbf{k}\cdot\mathbf{x}-\omega t)}$ and $\delta m_z = A_z e^{i(\mathbf{k}\cdot\mathbf{x}-\omega t)}$ we see

$$\begin{aligned} -i\hbar\omega A_y &= -(J|\mathbf{k}|^2 + K_x + B)A_z - iDk_y A_y, \\ -i\hbar\omega A_z &= (J|\mathbf{k}|^2 + K_x + B)A_y + iDk_y A_z, \end{aligned}$$

which leads to

$$\begin{pmatrix} i\hbar\omega - iDk_y & -(J|\mathbf{k}|^2 + K_x + B) \\ (J|\mathbf{k}|^2 + K_x + B) & i\hbar\omega - iDk_y \end{pmatrix} \begin{pmatrix} A_y \\ A_z \end{pmatrix} = \begin{pmatrix} 0 \\ 0 \end{pmatrix},$$

which gives us the dispersion relation

$$\hbar\omega = J|\mathbf{k}|^2 + Dk_y + K_x + B. \tag{2.3}$$

This relation is very similar to Eq. 2.2, but also has a term that is linear in k_y. The value of D does not effect the (ω, k_x) dispersion relation, which is similar to the (ω, k_x) dispersion relation of the axial regime. The (ω, k_y) dispersion relation is plotted in Fig. 2.4. In the (ω, k_y) dispersion relation, a nonzero magnetic field is assumed. This leads to the appearance of a 'gap", as discussed before. Increasing DMI leads to the minimum (as well as the rest of the parabola that is the dispersion relation) moving downward (i.e. the 'gap' closing again) and to the left. Physically, this means that, with a nonzero DMI, a spin wave can assume an energy level that, without DMI, was inside the gap. At low energy (e.g. ultracold temperatures), a small increase in energy can therefore lead to excited states that would not appear without the presence of DMI. In this case, the k_y-component needs to be negative. Also, its frequency will be lower than that of the lowest excited state without DMI. Analogously, for a spin wave to reach an excited state with positive k_y, a greater amount of energy is needed than without DMI, and a greater frequency will be observed.

Furthermore, as we can see in 2.4a, for some combinations of the values of B, K_x and D, the minimum has an ω-value lower than zero. In this case, the normal ground state of the system becomes unstable, and we are likely to end up with a spiraling state, as discussed earlier in section 1.3. In this state, the influence of the DM-Interaction is manifest (see Fig. 1.5). We denote the value of D for which this happens by D_{crit}. A straightforward calculation tells us $D_{crit} = 2\sqrt{J(B + K_x)}$.

2.2 Expanding the Landau-Lifshitz equation

We now consider the same situation, but we add more terms to the Landau-Lifshitz equation: the Gilbert damping term, and two terms concerning spin orbit torques (SOT's). The expanded Landau-Lifshitz-Gilbert equation with SOT's looks like this:

$$\hbar\partial_t \mathbf{m} = -\mathbf{m} \times \frac{\delta E}{\delta \mathbf{m}} - \alpha_G \mathbf{m} \times \hbar\frac{d\mathbf{m}}{dt} + a_j[\mathbf{m} \times (\hat{z} \times \mathbf{j})] + b_j[\mathbf{m} \times (\mathbf{m} \times (\hat{z} \times \mathbf{j}))]. \tag{2.4}$$

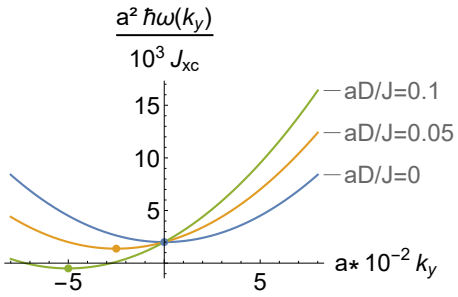

(a) The (ω, k_y) dispersion relation for different values of D. As D increases, the minimum can become smaller than zero, leading to an unstable ground state.

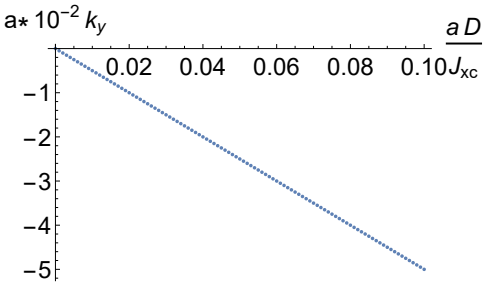

(b) The k_y-value of the minimum of the dispersion relation, as a function of D.

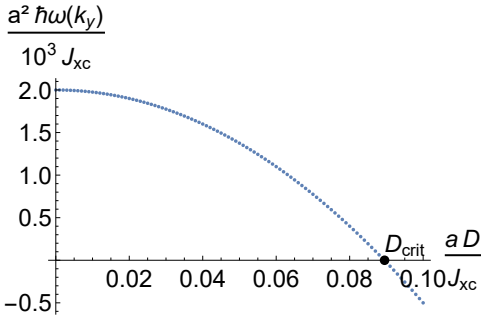

(c) The ω-value of the minimum of the dispersion relation, as a function of D. At D_{crit}, whose value also depends on B and K_x, the groundstate becomes unstable.

Figure 2.4 – The effect of D on the (ω, k_y) dispersion relation in the planar regime, with $\frac{a^2 K_z}{J} = \frac{a^2 B}{J} = 10^{-3}$. A larger value of D causes the minimum to shift to the left and downward. A higher value of B and K_x cause the entire parabola to shift upward (a larger 'gap'), in a way that is analogous to Fig. 2.3.

The second term, the one with α_G, is called the Gilbert damping term. It governs the equations of motion in such a way that deviations from the equilibrium will die out over time, as discussed in chapter 1 (see Fig. 1.3). The third and fourth term, with a_j and b_j, concern SOT's. SOT's are a consequence of the injection of an electric current $\mathbf{j}$ into the 2D-plane, which induces a spin accumulation component transverse to the current, as well as a longitudinal one that rotates[29]. The term proportional to a_j is also called the *spin-transfer torque*, *in-plane torque* or *anti-damping torque*. The term proportional to b_j is also called the *perpendicular torque*, *out-of-plane torque* or *field-like torque*. The constants a_j and b_j depend on factors like the current $\mathbf{j}$, the magnetization and the materials. If $\mathbf{j}$ is chosen in a specific way, the Gilbert damping term can be cancelled. In the computation of the transverse and longitudinal spin currents in chapter 3, we will not consider SOT's.

2.2.1 Linearzing around an axial equilibrium

In the axial regime ($\mathbf{B} = B\hat{z}$), we will not look at SOT's, as their contribution will cause problems when linearizing: the linearized contribution of the SOT's has no contributions that are linear in $\mathbf{m}$. Taking, again, $\mathbf{m} = (\delta m_x, \delta m_y, 1)^T$, and applying Eq. 2.4 we find

$$\begin{aligned} \hbar\partial_t(\delta m_x) &= (B + K_z - J\nabla^2 + \alpha_G\hbar\partial_t)\delta m_y, \\ \hbar\partial_t(\delta m_y) &= -(B + K_z - J\nabla^2 + \alpha_G\hbar\partial_t)\delta m_x. \end{aligned}$$

Taking Ansatzes $\delta m_x = A_x e^{i(\mathbf{k}\cdot\mathbf{x}-\omega t)}$ and $\delta m_y = A_y e^{i(\mathbf{k}\cdot\mathbf{x}-\omega t)}$ we find

$$\begin{aligned} -i\hbar\omega A_x &= (B + K_z + J|\mathbf{k}|^2 - i\alpha_G\hbar\omega)A_y, \\ -i\hbar\omega A_y &= -(B + K_z + J|\mathbf{k}|^2 - i\alpha_G\hbar\omega)A_x, \end{aligned}$$

and thus

$$\begin{pmatrix} i\hbar\omega & (B + K_z + J|\mathbf{k}|^2 - i\alpha_G\hbar\omega) \\ -(B + K_z + J|\mathbf{k}|^2 - i\alpha_G\hbar\omega) & i\hbar\omega \end{pmatrix} \begin{pmatrix} A_x \\ A_y \end{pmatrix} = \begin{pmatrix} 0 \\ 0 \end{pmatrix},$$

which yields, neglecting α_G^2, as $\alpha_G^2 \ll 1$, the dispersion relation

$$\hbar\omega = -i\alpha_G(B + K_z + J|\mathbf{k}|^2) + (B + K_z + J|\mathbf{k}|^2). \tag{2.5}$$

The effect of the damping term on the imaginary part of the dispersion relation is shown in Fig. 2.5.

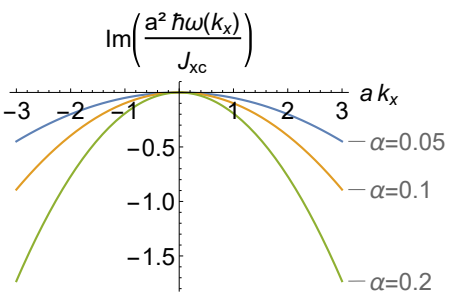

(a) Effect of α on (ω, k_x) dispersion relation.

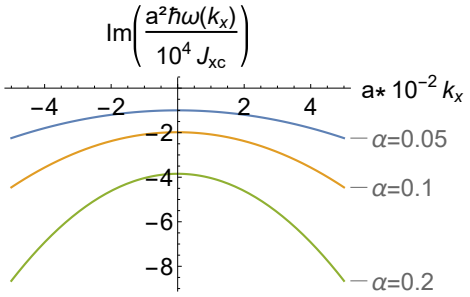

(b) Effect of α on (ω, k_x) dispersion relation, zoomed in.

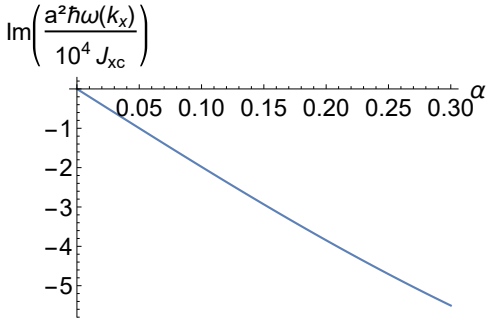

(c) The ω-coordinate of the maximum of the dispersion relation as a function of α

Figure 2.5 – The imaginary part of the (ω, k_x) dispersion relation in the axial regime ($\mathbf{B} = B\hat{z}$) for different values of α_G, with $\frac{a^2 B}{J} = \frac{a^2 K_z}{J} = 10^{-3}$ and $K_x = 0$. Due to rotational symmetry, the (ω, k_y) dispersion relation looks the same.

In this relation we assumed $\mathbf{k}$ to be real and left room for ω to be complex. If we view the effect of ω being complex ($\omega = \omega_r + i\omega_i$), the Ansatz will look like $\delta m_x = A_x e^{i(\mathbf{k}\ \mathbf{x} - \omega_r t)} e^{\omega_i t}$. If ω_i is negative, like in Eq. 2.5, the Ansatz will approach zero as time increases. We can thus view the complex part of ω as a term that damps the excitation of a system. A complex ω thus governs the excitation of an entire system that simultaneously damps over time.

We could also solve the relation by assuming that ω is real and $\mathbf{k}$ is complex ($\mathbf{k} = \mathbf{k}_r + i\mathbf{k}_i$). If we enter this into the Ansatz, we see $\delta m_x = A_x e^{i(\mathbf{k}_r \mathbf{x} - \omega t)} e^{-\mathbf{k}_i \mathbf{x}}$. We can also write $\mathbf{k}_i = \frac{1}{\Lambda}$. This way, the effect on the Ansatz looks very suggestive: $\delta m_x = A_x e^{i(\mathbf{k}_r \mathbf{x} - \omega t)} e^{-\frac{\mathbf{x}}{\Lambda}}$. We can see that Λ governs the length scale over which the excitation will die out. Using a complex $\mathbf{k}$ corresponds to viewing a local excitation of a system, with this excitation damping as it gets further from the point of excitation. Λ is sometimes referred to as the *relaxation distance*[14]. We can calculate Λ, and we find that, in the x-direction of propagation,

$$\Lambda_x = 2\frac{\sqrt{J(\hbar\omega - (B + K_z))}}{\hbar\omega\alpha}. \tag{2.6}$$

This formula has some interesting properties that are clarified in Fig. 2.6, where we can see Λ_x as a function of ω. Fig. 2.6a shows us how Λ_x governs that when the system is excited locally, the excitation diminishes the further it gets from the point of excitement. Of course, the value of α_G influences the damping of the excitation. If we look at Fig. 2.6b, however, some additional properties of Λ_x can be seen. Firstly, it appears that Λ has no real value up to a certain value of ω, depending on the value of B. This is because there are no spin waves until ω exceeds a certain value. This value is what we have previously referred to as the 'gap'. Secondly, we see a rapid increase of the value of Λ, before its gradual decrease sets in. Obviously, Λ has a local maximum, which is something that, at first, may not be very intuitive. Λ, being the relaxation length, has a length dimension. It appears that Λ_x is proportional to $v_{\mathbf{k}}\tau_{\mathbf{k}}$, where $v_{\mathbf{k}}$ is the wave velocity defined by $v_{\mathbf{k}} = \frac{\partial(\hbar\omega(\mathbf{k}))}{\partial\mathbf{k}}$ and $\tau_{\mathbf{k}}$ is the *relaxation time* defined by $\tau_{\mathbf{k}} = \frac{1}{\alpha\omega(\mathbf{k})}$. As $v_{\mathbf{k}}$ is linear in this case, knowing $\omega(\mathbf{k})$, a maximum is to be expected.

2.2.2 Linearzing around a planar equilibrium

It turns out it does make sense to include part of the spin-orbit torque term in the planar regime ($\mathbf{B} = B\hat{x}$), by setting $\mathbf{j} = (0, j, 0)^T$. We use Eq. 2.4 to find

$$\begin{aligned}
\hbar\partial_t(\delta m_y) &= -(-J\nabla^2 + B + K_x + \alpha_G\hbar\partial_t - a_j j)\delta m_z + (-D\partial_y + b_j j)\delta m_y, \\
\hbar\partial_t(\delta m_z) &= (-J\nabla^2 + B + K_x + \alpha_G\hbar\partial_t - a_j j)\delta m_y + (-D\partial_y + b_j j)\delta m_z.
\end{aligned}$$

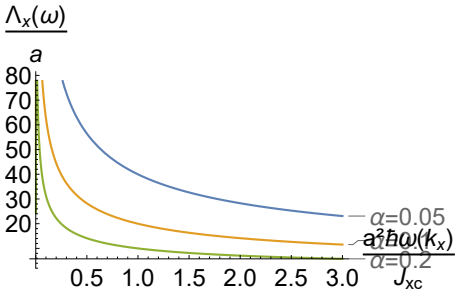

(a) Effect of α on the (Λ_x, ω) relation, with $\frac{a^2 B}{J} = \frac{a^2 K_x}{J} = 10^{-3}$ and $K_z = 0$.

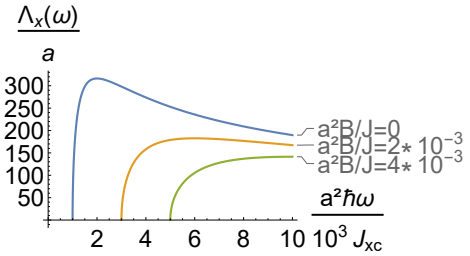

(b) The effect of B on the (Λ_x, ω) relation, with $\frac{a^2 B}{J} = 10^{-3}, K_z = 0$ and $\alpha = 0.1$.

Figure 2.6 – The behaviour of Λ_x for different values of α and B in the axial regime ($\mathbf{B} = B\hat{z}$). Note the scale difference on the axes.

Taking Ansatzes $\delta m_y = A_y e^{i(\mathbf{k}\cdot\mathbf{x}-\omega t)}$ and $\delta m_z = A_z e^{i(\mathbf{k}\cdot\mathbf{x}-\omega t)}$ we see

$$\begin{aligned} -i\hbar\omega A_y &= -(\mu(\mathbf{k}) - i\alpha_G\hbar\omega)A_z + \nu(\mathbf{k})A_y, \\ -i\hbar\omega A_z &= (\mu(\mathbf{k}) - i\alpha_G\hbar\omega)A_y + \nu(\mathbf{k})A_z, \end{aligned}$$

where $\mu(\mathbf{k}) \equiv (J|\mathbf{k}|^2 + B + K_x - a_j j)$ and $\nu(\mathbf{k}) \equiv (-iDk_y + b_j j)$. This leads to

$$\begin{pmatrix} i\hbar\omega + \nu(\mathbf{k}) & -(\mu(\mathbf{k}) - i\alpha_G\hbar\omega) \\ (\mu(\mathbf{k}) - i\alpha_G\hbar\omega) & i\hbar\omega + \nu(\mathbf{k}) \end{pmatrix} \begin{pmatrix} A_y \\ A_z \end{pmatrix} = \begin{pmatrix} 0 \\ 0 \end{pmatrix}.$$

As $\alpha_G^2 \ll 1$, we can neglect it. This yields the dispersion relation

$$\hbar\omega = i[b_j j - \alpha_G(J|\mathbf{k}|^2 + B + K_x - a_j j)] + [(J|\mathbf{k}|^2 + Dk_y + B + K_x - a_j j) + \alpha_G(-iDk_y + b_j j)]. \tag{2.7}$$

In Fig. 2.7, the effect of the Gilbert damping term and spin-orbit torques on the imaginary part of the dispersion relation is shown. We see that the SOT-plots are straight lines with positive value, and the Gilbert damping plots are parabolas with negative value. We see that with a correctly chosen current $\mathbf{j}$, the damping of a certain frequency $\pm\omega$ is cancelled, as the inverted parabolas would intersect the straight lines twice. This would lead to a spin wave that doesn't die out over time for that particular ω.

In the same way as before, we can also solve the equation for k, where we consider ω to be real and k_x to be complex. This leads to

$$\Lambda_x = \frac{\sqrt{J(\hbar\omega - (B + K_x - a_j j))}}{\alpha\hbar\omega - b_j j}. \tag{2.8}$$

It is easy to see that this relation is the same as the one in Eq. 2.6 if we set $a_j = b_j = j = 0$, which will lead to the same plots as in Fig. 2.6. The effects of different values of a_j

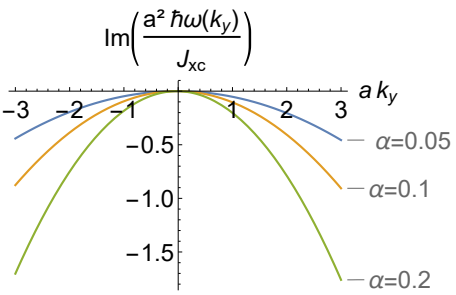

(a) The imaginary part of the (ω, k_y) dispersion relation in the planar regime, without SOT's, plotted for different values of α_G. The (ω, k_x) dispersion relation looks the same as Fig 2.5.

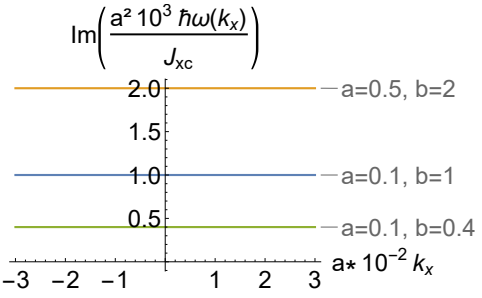

(b) The imaginary part of the (ω, k_x) dispersion relation in the planar regime, with SOT's, plotted for different values of a_j and b_j, with $j = 1$ and $\alpha_G = 0$.

Figure 2.7 – Effects of different values of α, b_j and a_j in the planar regime ($\mathbf{B} = B\hat{x}$). Plotted with $\frac{a^2 B}{J} = \frac{a^2 K_x}{J} = 10^{-3}$, $\frac{aD}{J} = 0.05$.

and b_j is shown in Fig. 2.8. We see that choosing a current strength $\mathbf{j}$ can lead to waves of certain frequencies being sustained (i.e. the damping is exactly cancelled), others to be amplified, as if an inverted damping process was taking place, and yet others to damp slower.

2.3 Linearizing around equilibria not coinciding with the external magnetic field

In the above chapter we took K_x and K_z to be zero in the axial regime and in the planar regime, respectively. If they are nonzero, the equilibrium may not be in the x- or z-direction. As there is a competition between the different anisotropies and the magnetic field interaction, the equilibrium will lie somewhere in the (x, z)-plane, as we saw in Fig. 2.2.

2.3.1 Linearizing around an equilibrium not coinciding with the magnetic field in the axial regime

In the axial regime ($\mathbf{B} = B\hat{z}$), an equilibrium that doesn't coincide with the z-direction only appears when $K_x > K_z + B$, as is shown in Fig. 2.9. When $K_x > K_z + B$, the equilibrium will make an angle with the z-axis of $\arccos(\frac{B}{K_x - K_z})$. The formulas resulting from solving this new set of equations are too long to make any intuitive sense.

In Fig. 2.10 the effect of increasing K_x on the real, undamped (ω, k_x) dispersion relation is plotted. A small but nonzero K_x in the axial regime leads to decreasing the gap between the minimum and zero created by K_z and B. After reaching the $K_x = K_z + B$

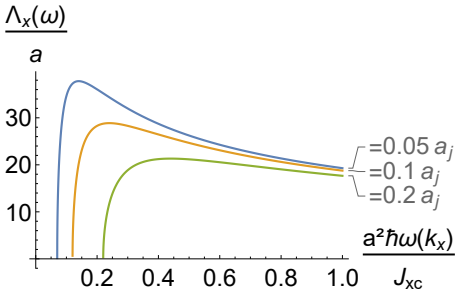

(a) Λ_x as a function of ω, for different values of $\frac{a_j}{j}$. Note that, although the plots look similar, the scale of ω is much larger than in Fig. 2.6b

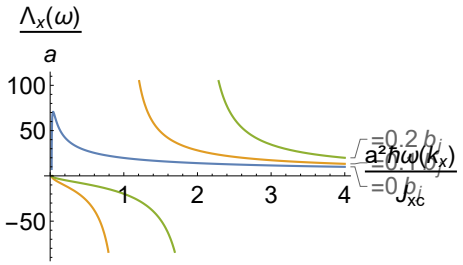

(b) Λ_x as a function of ω, for different values of $\frac{b_j}{j}$. Note that, for small values of ω, b_j actually amplifies the wave.

Figure 2.8 – Effects of a_j, b_j and j on the (Λ_x, ω) relation in the planar regime ($\mathbf{B} = B\hat{x}$), with $\frac{a^2 B}{J} = \frac{a^2 K_x}{J} = 10^{-3}$and $\alpha = 0.1$.

treshold, a larger K_x leads to the gap growing again. This means that, for a small increase in K_x, less energy is needed to reach the lowest excited state. At the treshold, the gap disappears, leading to a gapless dispersion relation. This means that the lowest excited state is the same as the vacuum state, and that any nonzero amount of energy added to the system will result in an excited state.

It turns out that, at this treshold, the second order derivative of the dispersion relation with respect to $\mathbf{k}$ is equal to zero. Furthermore, the dispersion displays linear behaviour. A linear approximation of the dispersion relation at this treshold is

$$\hbar\omega \approx \sqrt{J(B + K_z)}|\mathbf{k}|, \tag{2.9}$$

where we, of course, could also have written $(B + K_z)$ instead of K_x. In Fig. 2.11a we can see what the dispersion relation looks like at this treshold. Its linearity around zero is manifest. In Fig. 2.12 we see the effect of increasing K_x on the real, undamped (ω, k_y) dispersion relation. In addition to the effects on the 'gap', which were discussed above, after reaching a the $K_x = K_z + B$ treshold, a larger K_x leads to the minimum moving to the left as well, as the DM-interaction will have its influence when the equilibrium doesn't coincide with the z-axis. This means that the lowest excited state will have a negative k_y-value and that more energy is needed to reach an excited state with a positive k_y-value.

Fig. 2.13 shows the effect of increasing K_x on the imaginary, damping part of the (ω, k_x) dispersion relation. Increasing K_x leads to the gap closing for small, nonzero K_x, and to the gap increasing once it passes the $K_x = K_z + B$ threshold. In Fig. 2.14 we see the effect of increasing K_x on the imaginary, damping part of the (ω, k_y) dispersion relation. Increasing K_x also leads to the gap closing for small, nonzero K_x, and to the gap increasing once it passes the $K_x = K_z + B$ threshold. In this case, after passing the threshold the minimum also moves to the left as a consequence of DMI.

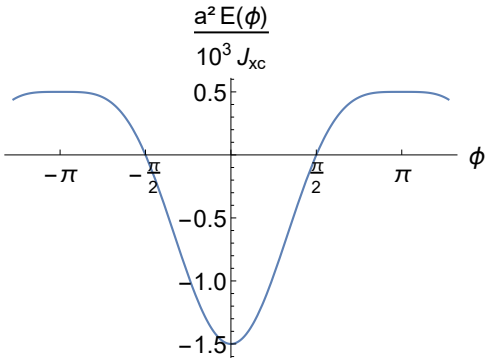

(a) For $K_x = 0$, we see a clear minimum at $\phi = 0$.

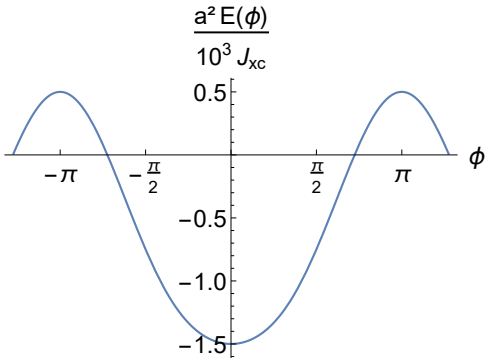

(b) If $K_x = K_z + B$, the minimum is still at $\phi = 0$, but deviations around the equilibrium will be larger, as they cost less energy.

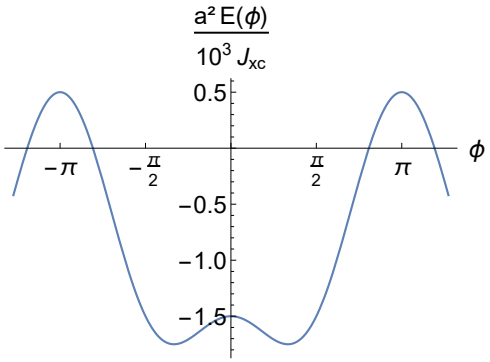

(c) When $K_x > K_z + B$ we see that the minimum of the free energy doesn't coincide with the z-axis.

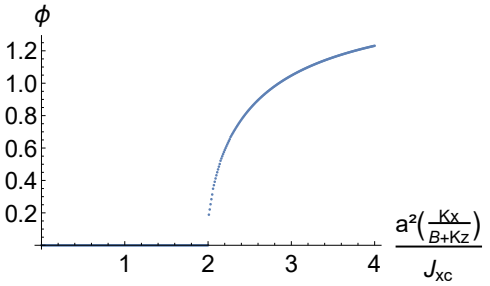

(d) The ϕ-value of the minimum, as a function of K_x. As soon as $K_x > K_z + B$, the equilibrium doesn't coincide with the z-axis.

Figure 2.9 – Free energy of the system in the axial regime ($\mathbf{B} = B\hat{z}$) as a function of the angle ϕ, where ϕ is the angle the equilibrium makes with the z-axis. Plotted with $\frac{a^2 K_z}{J} = \frac{a^2 B}{J} = 10^{-3}$.

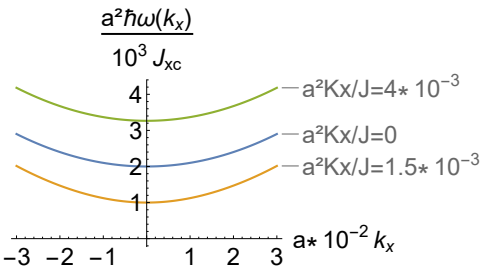

(a) (ω, k_x) dispersion relation, for $K_x = 0$, $0 < K_x < K_z + B$, and $K_x > K_z + B$.

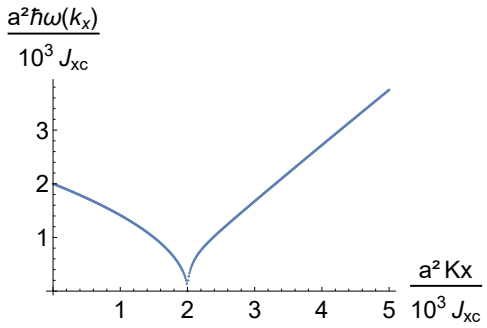

(b) The ω-value of the minimum as a function of K_x. A discontinuity at $K_x = K_z + B$ can be seen.

Figure 2.10 – Effect of K_x on the (ω, k_x) dispersion relation in the axial regime ($\mathbf{B} = B\hat{z}$). Plotted with $\frac{a^2 B}{J} = \frac{a^2 K_z}{J} = 10^{-3}$.

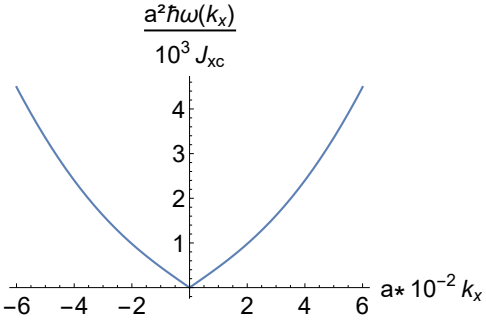

(a) (ω, k_x) dispersion relation in the axial regime ($\mathbf{B} = B\hat{z}$), for $K_x = K_z + B$. Due to rotational symmetry, the (ω, k_y) dispersion relation looks the same.

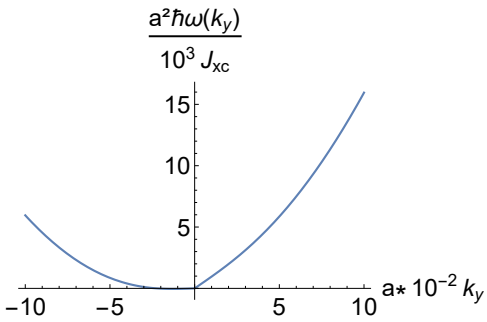

(b) (ω, k_y) dispersion relation in the planar regime ($\mathbf{B} = B\hat{x}$), for $K_z = K_x + B$. The plot of the (ω, k_x) dispersion relation looks the same as Fig 2.11a.

Figure 2.11 – Effect of a specific value for K_x (left) and K_z (right). Plotted with $\frac{a^2 B}{J} = \frac{a^2 K_z}{J} = 10^{-3}$ and $\frac{aD}{J} = 0.05$.

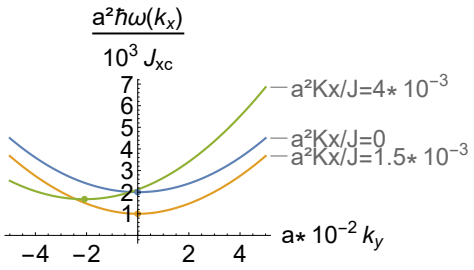

(a) The (ω, k_y) dispersion relation, for $K_x = 0$, $0 < K_x < K_z + B$, and $K_x > K_z + B$.

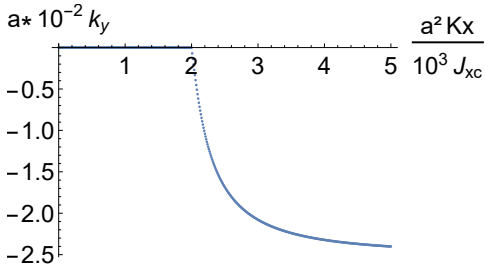

(b) The k_y-value of the minimum as a function of K_x. A discontinuity at $K_x = K_z + B$ can be seen.

Figure 2.12 – Effect of K_x on the (ω, k_y) dispersion relation in the axial regime ($\mathbf{B} = B\hat{z}$). Plotted with $\frac{a^2 B}{J} = \frac{a^2 K_z}{J} = 10^{-3}$ and $\frac{aD}{J} = 0.05$. The ω-value of the minimum as a function of K_x looks the same as Fig. 2.10b

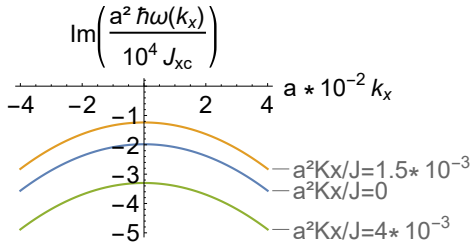

(a) Imaginary part of the (ω, k_x) dispersion relation, for $K_x = 0$, $0 < K_x < K_z + B$, and $K_x > K_z + B$.

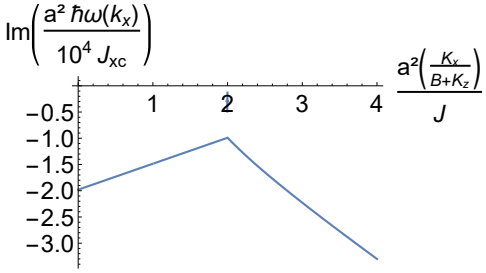

(b) The imaginary part of the ω-value of the minimum as a function of K_x.

Figure 2.13 – Effect of K_x on the imaginary part of the (ω, k_x) dispersion relation in the axial regime ($\mathbf{B} = B\hat{z}$). Plotted with $\frac{a^2 B}{J} = \frac{a^2 K_z}{J} = 10^{-3}$.

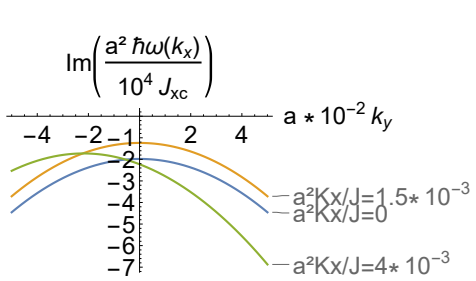

(a) Imaginary part of the (ω, k_x) dispersion relation, for $K_x = 0$, $0 < K_x < K_z + B$, and $K_x > K_z + B$.

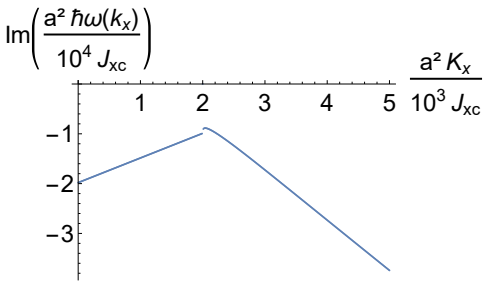

(b) The imaginary part of the ω-value of the minimum as a function of K_x.

Figure 2.14 – Effect of K_x on the imaginary part of the (ω, k_y) dispersion relation in the axial regime ($\mathbf{B} = B\hat{z}$). The plot of the k_y-value of the minimum as a function of K_x is the same as Fig. 2.12b. Plotted with $\frac{a^2 B}{J} = \frac{a^2 K_z}{J} = 10^{-3}$, $\frac{aD}{J} = 0.05, a_j = b_j = j = 0$ and $\alpha_G = 0.1$.

2.3.2 Linearizing around an equilibrium not coinciding with the magnetic field in the planar regime

In the planar regime ($\mathbf{B} = B\hat{x}$), an equilibrium that doesn't coincide with the x-axis only appears when $K_z > K_x + B$. The plots of the free energy will look the same as Fig. 2.9, where K_z and K_x should be substituted, and the ϕ-value of the minimum will start off at $\frac{\pi}{2}$ and will start to move towards 0 once K_z passes the treshold $K_z = B + K_x$. When this is the case, the equilibrium will make an angle $\arcsin(\frac{B}{K_z - K_x})$ with the z-axis. Again, the formulas turn out to be too long to make any intuitive sense. It turns out that the effect of increasing K_z on the real, undamped (ω, k_x) dispersion relation is similar to the effect of increasing K_x on the real, undamped (ω, k_x) dispersion relation in the axial regime (see Fig. 2.10). Its linear approximation will be the same as in Eq. 2.9, where we, of course, substitute K_x with K_z. The effect on the real, undamped (ω, k_y) dispersion relation is shown in Fig. 2.15. Its linear approximation is

$$\hbar\omega \approx \sqrt{J(B + K_x)}|k_y| + Dk_y, \tag{2.10}$$

where we could have written K_z instead of $(B + K_x)$. In Fig. 2.11b we can see what the dispersion relation looks like at this treshold. Its linearity around zero is manifest. The effect of increasing K_z on the imaginary, damping part of the (ω, k_x) dispersion relation is similar to the effect of increasing K_x on the imaginary, damping part of the (ω, k_x) dispersion relation in the axial regime (see Fig. 2.13). In Fig. 2.16 the effect of increasing K_z on the imaginary, damping part of the (ω, k_y) dispersion relation is shown.

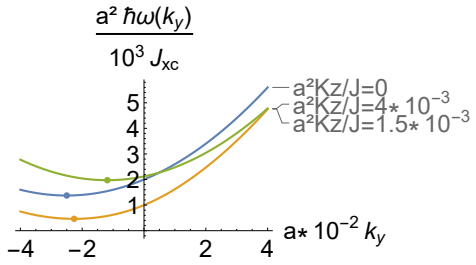

(a) (ω, k_y) dispersion relation, for $K_z = 0, 0 < K_z < K_x + B$ and $K_z > K_x + B$.

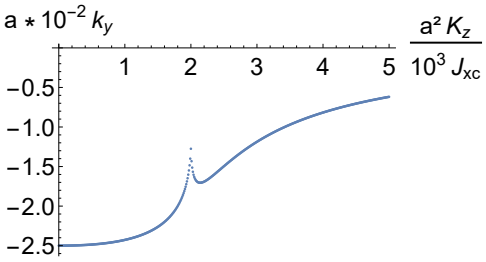

(b) k_y-coordinate of the minimum as a function of K_z. A discontinuity at $K_z = K_x + B$ can be seen.

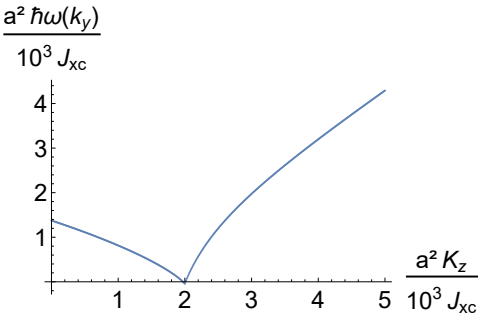

(c) The ω-value of the minimum as a function of K_z. A discontinuity at $K_z = K_x + B$ can be seen.

Figure 2.15 – The effect of increasing K_z in the planar regime ($\mathbf{B} = B\hat{x}$) has an effect on the ω-value of the minimum that can be somewhat expected, when comparing it to our results in the axial regime ($\mathbf{B} = B\hat{z}$), Fig. 2.10b. The effect on the k_y-coordinate is less intuitive. Plotted with $\frac{a^2 B}{J} = \frac{a^2 K_z}{J} = 10^{-3}$ and $\frac{aD}{J} = 0.05$.

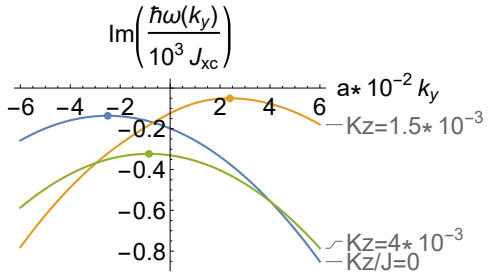

(a) Imaginary part of the (ω, k_y) dispersion relation, for $K_z = 0, 0 < K_z < K_x + B$ and $K_z > K_x + B$.

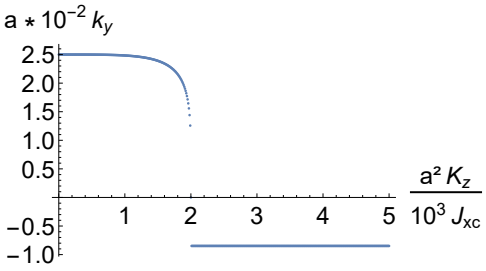

(b) k_y-coordinate of the minimum as a function of K_z. A discontinuity at $K_z = K_x + B$ can be seen.

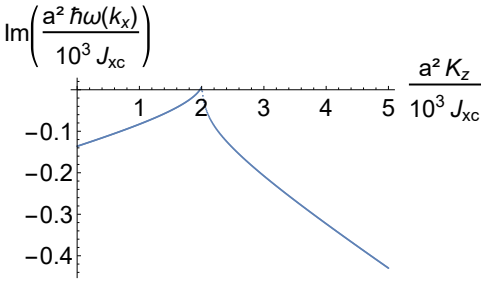

(c) ω-value of the maximum as a function of K_z. A discontinuity at $K_z = K_x + B$ can be seen.

Figure 2.16 – Increasing K_z in the planar regime ($\mathbf{B} = B\hat{x}$) has an expected effect on the ω-value of the minimum, but a less intuitive effect on its k_y-value. Plotted with $\frac{a^2 B}{J} = \frac{a^2 K_x}{J} = 10^{-3}$, $\frac{aD}{J} = 0.05, a_j = b_j = j = 0$ and $\alpha_G = 0.1$.

2.4 Consequences for our setup

We see that different ratios of the four interactions can have different, far-reaching consequences. First off, the influence of increasing the external magnetic field is the same as increasing the anisotropy term that points in the same direction as the external magnetic field. Both lead to the appearance of a 'gap' in the dispersion relation. Physically, this means that the lowest excited state has a greater energy and frequency than without the 'gap'. It is therefore impossible to find magnons with an energy level between the vacuum state and the first excited state. A greater amount of energy is thus needed to have a spin wave 'jump' to its lowest excited state. In a system of spins at zero temperature with a large external magnetic field, adding a small amount of energy, like a small increase in temperature or a moving electron (i.e. a small injected electric current), will therefore not lead to any excitations in the system, as the 'gap' will not be overcome by these small energy increases.

DMI only has linear contributions if the equilibrium is chosen not to be in the z-direction. This makes sense, as DMI was defined to operate in a plane perpendicular to the z-direction. We thus expect to see that an axial equilibrium will lead to a vanishing transverse current when we linearize each contribution to the Hamiltonian. An appropriately chosen equilibrium direction, such as $\hat{x}$, is therefore crucial if we want to perform our calculation. Furthermore, for large values of DMI strength with respect to the magnetic field and the anisotropy term coinciding with the magnetic field, the ground state becomes unstable. This would lead to a spiraling groundstate. In our setup, we choose an external magnetic field for which this does not happen.

We also saw that, assuming a nonzero magnetic field, increasing DMI strength leads to a decrease of the magnitude of the 'gap' in the $\omega - k_y$ dispersion relation, as well as a shift of the minimum (and the rest of the dispersion relation) to the left. Physically, this means that, with a nonzero DMI, a spin wave can assume an energy level that, without DMI, was inside the gap. At low energy, a small increase in energy can therefore lead to excited states that would not appear without the presence of DMI. In this case, the k_y-component needs to be negative, making the asymmetric influence of DMI manifest. Also, its frequency will be lower than that of the lowest excited state without DMI. Analogously, for a spin wave to reach an excited state with positive k_y, a greater amount of energy is needed than without DMI, and a greater frequency will be observed if this excited state is reached.

Increasing the anisotropy perpendicular to the magnetic field also has a big influence on the spin waves. For a small increase in K_x, less energy is needed to reach the lowest excited state, i.e. the 'gap' is diminished. If we keep increasing the perpendicular anisotropy, at a certain point, the 'gap' will close, leading to a gapless dispersion relation that displays linear behaviour around its minimum. This means that the lowest excited state is the same as the vacuum state, and that any nonzero amount of energy added to the system will result in an excited state. If we keep increasing the perpendicular anisotropy, we will see the influence of DMI in a similar way as described above.

Furthermore, a sufficiently large perpendicular anisotropy can lead to an equilibrium position of the spins that is not aligned with this magnetic field. Having such an equilibrium position has a very significant effect on the dispersion relation. We had to resort to Mathematica in order to calculate the dispersion relation. As the computations in the next chapter are already very involved with an equilibrium that does coincide with the magnetic field, it makes sense to choose a setup in which the external magnetic field is large enough to ensure that an anisotropy perpendicular to this field will not affect the equilibrium position of the spins.

In the setup in the next chapter, all these considerations will be taken into account. We also note that conventional experimental setups tend to employ a relatively large external magnetic field.

Chapter 3

Influence of DMI on Magnon Spin Currents

In this chapter we consider magnon transport. Our setup consists of a ferromagnetic medium through which spin waves propagate. We assume the medium to be bounded by normal metals (e.g. platinum) at $x = 0$ and $x = d$, with a spin accumulation $\boldsymbol{\mu'}$ at the $x = 0$-interface. The medium and its medium-metal interfaces are assumed to stretch from $-\infty$ to $+\infty$ in the y- and z-direction. An illustration of this setup is shown in Fig. 3.1.

As before, we consider exchange interaction, magnetic field interaction, anisotropy and DMI. We will let the magnitude of the external field be large enough for the contributions from the interactions that arise due to the anisotropies and the external magnetic field to be summarized by taking an effective field $\mathbf{H}$ in the same direction as the external magnetic field. In chapter 2, we saw that for an appropriately large magnetic field, the influence of the anisotropies can be accounted for in this way. We also assume that the effects of DMI at the interfaces are similar to those in the bulk.

In discussing the dynamics of the spin waves, we also include a stochastic term. This term simulates (thermal) fluctuations, which can then be taken into account. We assume these simulated fluctuations to be Gaussian distributed, enabling us to predict the behaviour of these fluctuations in the long run[30][31]. If we regard fluctuations at a certain point in our setup, we can predict their contribution to the overall transverse current by employing the fluctuation dissipation theorem (FDT). The FDT states that the linear response of a system to an external perturbation can be expressed in terms of fluctuation properties of the system in thermal equilibrium[33]. This can be expressed as follows:

$$\left\langle h^*(x,\mathbf{q},\omega)h(x',\mathbf{q}',\omega')\right\rangle = 2(2\pi)^3\alpha\frac{\hbar}{s}\frac{\hbar\omega}{\tanh\left[\frac{\hbar\omega}{2T}\right]}\delta(x-x')\delta(\mathbf{q}-\mathbf{q}')\delta(\omega-\omega').$$

Approximating this for small $\hbar\omega$ yields

$$\left\langle h^*(x,\mathbf{q},\omega)h(x',\mathbf{q}',\omega')\right\rangle = 4(2\pi)^3\alpha\frac{\hbar}{s}T\delta(x-x')\delta(\mathbf{q}-\mathbf{q}')\delta(\omega-\omega'), \tag{3.1}$$

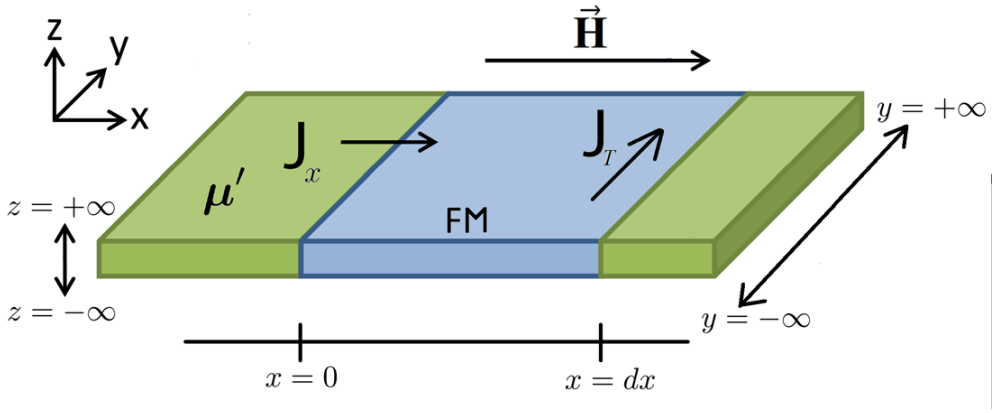

Figure 3.1 – A ferromagnet (FM) bounded by normal metals at $x = 0$ and $x = d$, together with an effective field $\mathbf{H} = H\hat{x}$ and a spin accumulation $\boldsymbol{\mu}'$, which leads to a longitudinal spin current J_L. If a transverse current J_T appears in the calculations, this would imply a prediction of the magnon Hall effect. Figure based on figure taken from [18].

which is the equation we will use from now on. We note that this stochastic term is not the most natural way to simulate magnon fluctuations, as magnons interacts with many degrees of freedom in the material. The stochastic term is added to the LLG equation, and we express it as

$$(1 + \alpha\mathbf{n}\times)\hbar\dot{\mathbf{n}} + \mathbf{n} \times (\mathbf{H} + \mathbf{h}) - A\mathbf{n} \times \nabla^2\mathbf{n} = 0. \tag{3.2}$$

Here, $\mathbf{H}$ is the effective field, $\mathbf{h}$ the stochastic field and A the exchange stiffness rather than J, which we used before. Also, we now use $\mathbf{n}$ rather than $\mathbf{m}$ now. Linearizing the LLG using $\mathbf{n} = (1, \delta n_y, \delta n_z)$, we find the equation of motion[1]

$$A(\partial_x^2 - \kappa^2)n = h, \tag{3.3}$$

where

$$\kappa^2 = |\mathbf{q}|^2 + \frac{H + Dq_y + (1 - i\alpha)\hbar\omega}{A}, \tag{3.4}$$

and $n \equiv n_y - in_z$ and $h \equiv h_y - ih_z$. We should note that, in the equation of motion, integrals over $d^2\mathbf{q}$ and $d\omega$, as well as powers of e have been omitted for brevity, after having appeared because of Fourier transforming in y, z and t. We will reintroduce them if necessary. A complete version of these equations can be found in Appendix A.

[1] A detailed calculation can be found in Appendix A.

At $x = 0$, the boundary condition without DMI contribution reads[2]

$$\mathbf{j}_s(x=0) = -As\mathbf{n} \times \partial_x \mathbf{n}|_{x=0} = -\left[\frac{g^{\uparrow\downarrow}}{4\pi}(\mathbf{n} \times (\mathbf{n} \times \boldsymbol{\mu}') + \mathbf{n} \times \hbar\dot{\mathbf{n}}) + \mathbf{n} \times \mathbf{h}'_L\right]_{x=0}, \quad (3.5)$$

whereas at $x = d$, the boundary condition without DMI contribution reads

$$\mathbf{j}_s(x=d) = -As\mathbf{n} \times \partial_x \mathbf{n}|_{x=d} = \left[\frac{g^{\uparrow\downarrow}}{4\pi}(\mathbf{n} \times \hbar\dot{\mathbf{n}}) + \mathbf{n} \times \mathbf{h}'_R\right]_{x=d}, \quad (3.6)$$

where we assume the spin accumulation $\boldsymbol{\mu}' = \mu'\hat{x}$ vanishes at the $x = d$-interface, and $\mathbf{h}'_L, \mathbf{h}'_R$ represent the stochastic terms at the left and right interface, respectively. Furthermore, s is the spin density, $g^{\uparrow\downarrow}$ is a mixing constant picked up at the interfaces, and the contribution of the effective field H vanishes at the boundaries.

Linearization tells us that the linearized DMI contribution vanishes at the boundaries, and that the linearized boundary conditions are

$$\left\{A\partial_x + i\frac{g^{\uparrow\downarrow}}{4\pi s}[\hbar\omega - \mu']\right\}\psi = \frac{h_L}{\sqrt{s}} \quad (3.7)$$

At x=0, and

$$\left\{A\partial_x - i\frac{g^{\uparrow\downarrow}}{4\pi s}\hbar\omega\right\}\psi = -\frac{h_R}{\sqrt{s}} \quad (3.8)$$

At x=d, where $\psi \equiv n\sqrt{s}$.

3.1 A solution for ψ at the interface

We want to to find a ψ that solves the boundary conditions from Eq. 3.7 and 3.8. We know that

$$\psi = \psi_B + \psi_I,$$

where ψ_B is a general solution for the bulk, and ψ_I is a particular solution of the boundary conditions at the interfaces.

We insert the Ansatz $\psi_I = C_1 e^{\kappa x} + C_2 e^{-\kappa x}$ into the boundary conditions from Eq. 3.7 and Eq. 3.8, where κ is defined in Eq. 3.4, as this Ansatz solves the equation of motion given by Eq. 3.3.

[2] A detailed calculation of this boundary condition and the following linearization can be found in Appendix B.

At $x = 0$ we have

$$\begin{aligned}\frac{h_L}{\sqrt{s}} &= A\kappa(C_1 - C_2) + i\frac{g^{\uparrow\downarrow}}{4\pi s}[\hbar\omega - \mu'](C_1 + C_2) \\ &= \left[A\kappa + i\frac{g^{\uparrow\downarrow}}{4\pi s}[\hbar\omega - \mu']\right] C_1 + \left[-A\kappa + i\frac{g^{\uparrow\downarrow}}{4\pi s}[\hbar\omega - \mu']\right] C_2 \\ &= \mathcal{A}C_1 + \mathcal{B}C_2,\end{aligned}$$

where we defined $\mathcal{A} \equiv \left[A\kappa + i\frac{g^{\uparrow\downarrow}}{4\pi s}[\hbar\omega - \mu']\right]$ and $\mathcal{B} \equiv \left[-A\kappa + i\frac{g^{\uparrow\downarrow}}{4\pi s}[\hbar\omega - \mu']\right]$. At $x = d$ we see

$$\begin{aligned}\frac{h_R}{\sqrt{s}} &= -A\kappa(C_1 e^{\kappa d} - C_2 e^{-\kappa d}) + i\frac{g^{\uparrow\downarrow}}{4\pi s}\hbar\omega(C_1 e^{\kappa d} + C_2 e^{-\kappa d}) \\ &= \left[-A\kappa + i\frac{g^{\uparrow\downarrow}}{4\pi s}\hbar\omega\right] C_1 e^{\kappa d} + \left[A\kappa + i\frac{g^{\uparrow\downarrow}}{4\pi s}\hbar\omega\right] C_2 e^{-\kappa d} \\ &= \mathcal{C}e^{\kappa d}C_1 + \mathcal{D}e^{-\kappa d}C_2,\end{aligned}$$

where we defined $\mathcal{C} \equiv \left[-A\kappa + i\frac{g^{\uparrow\downarrow}}{4\pi s}\hbar\omega\right]$ and $\mathcal{D} \equiv \left[A\kappa + i\frac{g^{\uparrow\downarrow}}{4\pi s}\hbar\omega\right]$. Combining these results leads to

$$\begin{pmatrix} \mathcal{A} & \mathcal{B} \\ \mathcal{C}e^{\kappa d} & \mathcal{D}e^{-\kappa d} \end{pmatrix} \begin{pmatrix} C_1 \\ C_2 \end{pmatrix} = \frac{1}{\sqrt{s}} \begin{pmatrix} h_L \\ h_R \end{pmatrix},$$

so that, finally,

$$\begin{pmatrix} C_1 \\ C_2 \end{pmatrix} = \frac{1}{\mathbb{D}} \begin{pmatrix} \mathcal{D}e^{-\kappa d} & -\mathcal{B} \\ -\mathcal{C}e^{\kappa d} & \mathcal{A} \end{pmatrix} \frac{1}{\sqrt{s}} \begin{pmatrix} h_L \\ h_R \end{pmatrix},$$

where $\mathbb{D} \equiv \mathcal{A}\mathcal{D}e^{-\kappa d} - \mathcal{B}\mathcal{C}e^{\kappa d}$

3.2 The transverse interfacial spin current

To compute the interfacial current in the y-direction, we use the formula[3]

$$\left\langle \hat{j}_y^{(I)}(x) \right\rangle = \left\langle \psi^*(x)\frac{\hat{v}_{q,y}}{2}\psi(x) \right\rangle,$$

[3] A motivation this formula and the following computation of the transverse interfacial current can be found in Appendix C.

where $\hat{v}_{q,y} = \frac{\partial \hbar\omega_{\mathbf{q}}}{\partial q_y}$. We use the dispersion relation from Eq. 2.3 to see that

$$\left\langle \hat{j}_y^{(I)}(x) \right\rangle = (Aq_y + \frac{D}{2}) \left\langle \psi^*(x)\psi(x) \right\rangle .$$

Computations lead to

$$\begin{aligned}
\langle \psi^*\psi \rangle = \; & \tfrac{16 g^{\uparrow\downarrow} \hbar T}{4\pi \mathbb{D}^* \mathbb{D} s} \Bigg[\; A^2 \kappa^* \kappa \cosh[\kappa^*(d-x)] \cosh[\kappa(d-x)] \\
& -iA\kappa^* \frac{g^{\uparrow\downarrow}}{4\pi s} \hbar\omega \cosh[\kappa^*(d-x)] \sinh[\kappa(d-x)] \\
& +iA\kappa \frac{g^{\uparrow\downarrow}}{4\pi s} \hbar\omega \sinh[\kappa^*(d-x)] \cosh[\kappa(d-x)] \\
& + \left(\frac{g^{\uparrow\downarrow}}{4\pi s} \hbar\omega \right)^2 \sinh[\kappa^*(d-x)] \sinh[\kappa(d-x)] \\
& +A\kappa^* \kappa \cosh[\kappa^* x] \cosh[\kappa x] \\
& -iA\kappa^* \frac{g^{\uparrow\downarrow}}{4\pi s} [\hbar\omega - \mu'] \cosh[\kappa^* x] \sinh[\kappa x] \\
& +iA\kappa \frac{g^{\uparrow\downarrow}}{4\pi s} [\hbar\omega - \mu'] \sinh[\kappa^* x] \cosh[\kappa x] \\
& + \left(\frac{g^{\uparrow\downarrow}}{4\pi s} [\hbar\omega - \mu'] \right)^2 \sinh[\kappa^* x] \sinh[\kappa x] \Bigg] .
\end{aligned}$$

Noting that D only enters into $\langle \psi^*\psi \rangle$ through κ, we now redefine $q_y \to \tilde{q}_y = q_y + \frac{D}{2A}$ so that

$$\kappa^2 = \tilde{q}_y^2 + q_z^2 - \left(\frac{D}{2A} \right)^2 + \frac{H + (1 - i\alpha)\hbar\omega}{A}.$$

We see that κ is symmetric under $\tilde{q}_y \to -\tilde{q}_y$. This leads to $\langle \psi^*\psi \rangle$ being symmetric under this transformation as well. We know that

$$\left\langle \hat{j}_y^{(I)} \right\rangle = (Aq_y + \frac{D}{2}) \left\langle \psi^*\psi \right\rangle = A\tilde{q}_y \left\langle \psi^*\psi \right\rangle ,$$

where, of course, we still have to integrate over $\tilde{q}_y$ to end up with the current (and q_z and ω, but those are not important for now). Obviously, $2A\tilde{q}_y$ is antisymmteric under $\tilde{q}_y \to -\tilde{q}_y$. Knowing that $\langle \psi^*\psi \rangle$ is symmetric, we see that upon integrating over $\tilde{q}_y$, $\left\langle \hat{j}_y^{(I)} \right\rangle$ vanishes.

3.3 A solution for ψ in the bulk

As before, we know

$$\psi = \psi_B + \psi_I,$$

where ψ_B is a general solution for the bulk, and ψ_I is a particular solution of the boundary conditions at the interfaces. To find ψ_B, we make use of the equation of motion (Eq. 3.3), the fluctuation dissipation theorem (Eq. 3.1) and the bulk boundary conditions, which are similar to the interfacial boundary conditions (Eq. 3.7 and Eq. 3.8) but with $h_L = h_R = 0$. Furthermore, we make use of

$$\psi(x) = \int_0^d dy G(x,y)\psi(y) = \int_0^d dy G(x,y)\frac{\sqrt{s}}{A}h(y), \tag{3.9}$$

where the second equality is due to the equation of motion and where

$$(\partial_x^2 - \kappa^2)G(x,y) = \delta(x-y).$$

We now integrate this:

$$\int_{y-\epsilon}^{y+\epsilon} dx(\partial_x^2 - \kappa^2)G(x,y) = \int_{y-\epsilon}^{y+\epsilon} dx\delta(x-y) = 1.$$

If we let $\epsilon \to 0$, we can conclude

$$(\partial_x G^> - \partial_x G^<)|_{x=y} = 1. \tag{3.10}$$

Defining $G^<(x,y)$ as the Green's function for $x \leq y$ and $G^>(x,y)$ as the Green's function for $x \geq y$, we use Ansatz

$$G(x,y) = \begin{cases} G^<(x,y) = ae^{\kappa x} + be^{-\kappa x} & \text{for } x < y \\ G^>(x,y) = \tilde{a}e^{\kappa x} + \tilde{b}e^{-\kappa x} & \text{for } x > y, \end{cases}$$

where, of course

$$G^<(x=y) = G^>(x=y), \tag{3.11}$$

with boundary conditions

$$\left\{A\partial_x + i\frac{g^{\uparrow\downarrow}}{4\pi s}[\hbar\omega - \mu']\right\}\psi = 0 \text{ at } x = 0,$$

and

$$\left\{A\partial_x - i\frac{g^{\uparrow\downarrow}}{4\pi s}\hbar\omega\right\}\psi = 0 \text{ at } x = d. \tag{3.12}$$

After some calculations,[4] we find

$$a = \frac{\sigma}{2\kappa}\left(\frac{\tilde{\sigma}^{-1}e^{-2\kappa d}e^{\kappa y} + e^{-\kappa y}}{\tilde{\sigma}^{-1}e^{-2\kappa d} - \sigma}\right),$$

$$b = \frac{1}{2\kappa}\left(\frac{\tilde{\sigma}^{-1}e^{-2\kappa d}e^{\kappa y} + e^{-\kappa y}}{\tilde{\sigma}^{-1}e^{-2\kappa d} - \sigma}\right),$$

$$\tilde{a} = \frac{\tilde{\sigma}^{-1}e^{-2\kappa d}}{2\kappa}\left(\frac{\sigma e^{\kappa y} + e^{-\kappa y}}{\tilde{\sigma}^{-1}e^{-2\kappa d} - \sigma}\right),$$

$$\tilde{b} = \frac{1}{2\kappa}\left(\frac{\sigma e^{\kappa y} + e^{-\kappa y}}{\tilde{\sigma}^{-1}e^{-2\kappa d} - \sigma}\right),$$

where

$$\sigma \equiv \frac{A\kappa - i\frac{g^{\uparrow\downarrow}}{4\pi s}[\hbar\omega - \mu']}{A\kappa + i\frac{g^{\uparrow\downarrow}}{4\pi s}[\hbar\omega - \mu']} = -\frac{\mathcal{B}}{\mathcal{A}},$$

and

$$\tilde{\sigma}^{-1} \equiv \frac{A\kappa + i\frac{g^{\uparrow\downarrow}}{4\pi s}\hbar\omega}{A\kappa - i\frac{g^{\uparrow\downarrow}}{4\pi s}\hbar\omega} = -\frac{\mathcal{D}}{\mathcal{C}}.$$

3.4 The transverse bulk spin current

We use the formula from section 3.2:

$$\left\langle \hat{j}_y^{(B)} \right\rangle = (Aq_y + \frac{D}{2}) \left\langle \psi^*(x)\psi(x) \right\rangle .$$

We set out to compute $\langle \psi^*(x)\psi(x)\rangle$. Using Eq. 3.9 leads to

$$\langle \psi^*(x)\psi(x)\rangle = \left\langle \left[\int_0^d dz G(x,z)\frac{\sqrt{s}}{A}h(z)\right]^* \left[\int_0^d dy G(x,y)\frac{\sqrt{s}}{A}h(y)\right]\right\rangle .$$

[4] A detailed version of these calculations can be found in Appendix D

Using the Ansatz

$$G(x,y) = \begin{cases} G^{<}(x,y) = ae^{\kappa x} + be^{-\kappa x} & \text{for } x < y \\ G^{>}(x,y) = \tilde{a}e^{\kappa x} + \tilde{b}e^{-\kappa x} & \text{for } x > y \end{cases}$$

with the values obtained in the previous chapter, we set out to perform some heavy calculations[5]. We end up with a formula for the transverse bulk current:

$$\begin{aligned}
\left\langle j_y^{(B)} \right\rangle = \mathrm{Im}\Bigg[(Aq_y + \frac{D}{2})\tilde{\Omega}\tilde{\beta}_1 \Bigg(\quad & A^2\kappa^*\kappa \quad \Big\{ \kappa \Big[\sinh[\kappa x]\cosh[\kappa^* x] \Big] \Big\} \\
& +\chi A\kappa \quad \Big\{ \kappa \Big[\sinh[\kappa x]\sinh[\kappa^* x] \Big] \\
& \qquad -\kappa^* \Big[\cosh[\kappa x]\cosh[\kappa^* x] \Big] + \kappa^* \Big\} \\
& +\chi^2 \quad \Big\{ -\kappa \Big[\cosh[\kappa x]\sinh[\kappa^* x] \Big] \Big\} \Bigg) \\
+(Aq_y + \frac{D}{2})\tilde{\Omega}\tilde{\beta}_2 \Bigg(\quad & A^2\kappa^*\kappa \quad \Big\{ \kappa \Big[\sinh[\kappa(d-x)]\cosh[\kappa^*(d-x)] \Big] \Big\} \\
& +\xi A\kappa \quad \Big\{ \kappa \Big[\sinh[\kappa(d-x)]\sinh[\kappa^*(d-x)] \Big] \\
& \qquad -\kappa^* \Big[\cosh[\kappa(d-x)]\cosh[\kappa^*(d-x)] \Big] + \kappa^* \Big\} \\
& +\xi^2 \quad \Big\{ -\kappa \Big[\cosh[\kappa(d-x)]\sinh[\kappa^*(d-x)] \Big] \Big\} \Bigg) \Bigg],
\end{aligned}$$

where

$$\begin{aligned}
\chi &\equiv i\frac{g^{\uparrow\downarrow}}{4\pi s}[\hbar\omega - \mu'], \\
\xi &\equiv i\frac{g^{\uparrow\downarrow}}{4\pi s}\hbar\omega, \\
\tilde{\Omega} &\equiv \int \frac{d^2\mathbf{q}}{(2\pi)^2} \int \frac{d\omega}{2\pi} \frac{-4T}{\omega A\kappa^*\kappa} \frac{1}{\mathbb{D}^*\mathbb{D}} m \\
\tilde{\beta}_1 &\equiv A^2\kappa^*\kappa \Big(\cosh[\kappa^*(d-x)]\cosh[\kappa(d-x)] \Big) + \xi^2 \Big(\sinh[\kappa^*(d-x)]\sinh[\kappa(d-x)] \Big), \\
\tilde{\beta}_2 &\equiv A^2\kappa^*\kappa \Big(\cosh[\kappa^* x]\cosh[\kappa x] \Big) + \chi^2 \Big(\sinh[\kappa^* x]\sinh[\kappa x] \Big).
\end{aligned}$$

[5] These can be found in Appendix E.

We now follow the same reasoning as with the interfacial transverse current $\left\langle \hat{j}_y^{(I)} \right\rangle$. If we define $\tilde{q}_y \equiv q_y + \frac{D}{2A}$, we can split up the formula for the current in a part that is antisymmetric under $\tilde{q}_y \to -\tilde{q}_y$ (the part which previously was $(Aq_y + \frac{D}{2})$) and a part that is symmetric under $\tilde{q}_y \to -\tilde{q}_y$ (the rest), as κ is symmetric under this transformation. This leads to the bulk current vanishing as well upon integration over $\tilde{q}_y$.

3.5 The longitudinal spin current evaluated at $x = d$

The vanishing result of the transverse current leads us to investigate whether there is any influence of DMI in the longitudinal spin current. We therefore do a less extensive computation of the longitudinal current by evaluating it at $x = d$.[6] We use the formula[7]

$$\left\langle \hat{j}_x(x) \right\rangle = A\mathrm{Im}[\langle \psi^* \partial_x \psi \rangle]_d.$$

Using the same shorthand notation as before, we see that the longitudinal interfacial current at $x = d$ equals

$$A \int \frac{d^2\mathbf{q}}{(2\pi)^2} \int \frac{d\omega}{2\pi} \mathrm{Im} \Bigg[16 \frac{g^{\uparrow\downarrow}}{4\pi s} \frac{\hbar T}{\mathbb{D}^* \mathbb{D}} \kappa \Bigg(\begin{array}{ll} \xi A \kappa^* & \\ +A^2 \kappa^* \kappa & \cosh[\kappa^* d] \sinh[\kappa d] \\ -\chi A \kappa^* & \cosh[\kappa^* d] \cosh[\kappa d] \\ +\chi A \kappa & \sinh[\kappa^* d] \sinh[\kappa d] \\ -\chi^2 & \sinh[\kappa^* d] \cosh[\kappa d] \end{array} \Bigg) \Bigg],$$

and that the longitudinal bulk current at $x = d$ equals

$$A \int \frac{d^2\mathbf{q}}{(2\pi)^2} \int \frac{d\omega}{2\pi} \mathrm{Im} \Bigg[-16 \frac{g^{\uparrow\downarrow}}{4\pi s} \frac{\hbar T}{\mathbb{D}^* \mathbb{D}} \kappa \Bigg(\begin{array}{ll} +\chi A \kappa^* & \\ A^2 \kappa^* \kappa & \sinh[\kappa x] \cosh[\kappa^* d] \\ +\chi A \kappa & \sinh[\kappa d] \sinh[\kappa^* d] \\ -\chi A \kappa^* & \cosh[\kappa d] \cosh[\kappa^* d] \\ +\chi^2 & -\cosh[\kappa d] \sinh[\kappa^* d] \end{array} \Bigg) \Bigg].$$

[6] A detailed calculation can be found in Appendix G.
[7] A motivation for this formula can be found in Appendix C.

Adding these together yields

$$\left\langle \hat{j}_x \right\rangle = A \int \frac{d^2\mathbf{q}}{(2\pi)^2} \int \frac{d\omega}{2\pi} 16 \left(\frac{g^{\uparrow\downarrow}}{4\pi s} \right)^2 \frac{\hbar T}{\mathbb{D}^* \mathbb{D}} A \kappa^* \kappa \mu'.$$

Here, D enters the equation through κ, as well as through $\mathbb{D}$. Even if we define $\tilde{q}_y$ as before, this would still have κ depending on D, which means that the longitudinal current depends on D either way. This shows that, in this setup, DMI does affect the spin current, even though a nonzero transverse spin current dependent on D is not predicted. We also see that the longitudinal spin current directly depends on μ', which makes intuitive sense. Without a magnon potential gradient, no spin current will appear in this setup.

Chapter 4

Conclusion and Outlook

Spintronics is a field of study that still has many open questions. One of the areas that has seen a lot of recent activity is the magnon Hall effect. In this thesis, we set out to do a theoretical examination of this effect as a consequence of DMI on electrically induced magnon spin currents. We introduced some basic concepts about spin waves in general, and DMI in particular. We saw that the ratios between the interaction constants of the Heisenberg exchange interaction, magnetic field interaction, anisotropy and DMI play a big part in the properties of the ground state and the dispersion relations. We then defined our setup in such a way that the contribution of the external magnetic field was bigger than that of the anisotropy and DMI, and pointed into the plane (our x-direction).

The magnon hall effect as a consequence of a spin current driven by a thermal gradient has been observed experimentally[14]. We know that a magnon spin current can also be driven electrically[14][19]. With an electrically driven spin current, intuition could lead us to expect a similar effect, especially in the presence of DMI. In our calculations, however, we ended up with a vanishing transverse current.

One of the reasons that the transverse current vanishes is that our calculation relies on linearization. If we regard our setup with an external magnetic field in the z-direction, we see that the DMI contribution vanishes upon linearization, making it impossible to examine DMI in this regime. In practice, DMI can definitely influence the setup, even if the external magnetic field is applied in the z-direction. We note that the experiment in which the thermally driven magnon Hall effect was measured employed an external magnetic field that was pointed in what we defined to be our $\hat{z}$-direction. Especially if the DMI constant D is large compared to the constants of the the external magnetic field and the anisotropies, we would expect to measure some influence of DMI. At second order, DMI does enter in this regime. Linearization is a tool often employed in physics, but it can have its drawbacks. We have seen in chapter 2 that the ratios of different interaction constants has a large effect on the dispersion relations, so we can assume that some significant effects may be lost when linearizing.

In our model, we also assumed that DMI affects the spins at the boundary in the same way that it affects the spins in the bulk. It has, however, been confirmed experimentally that, in certain materials, spin behaviour near the interfaces can be different from their behaviour in the bulk. In these materials, if we regard our setup and orient the equilibrium on the z-axis, DMI will cause the spins at the interfaces to point inward,

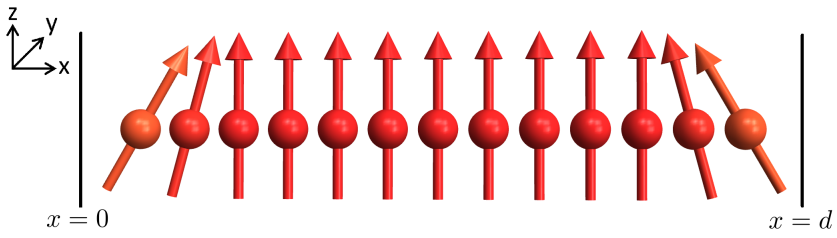

Figure 4.1 – In certain materials, the spins near the interface tend to point inward under the influence of DMI.

as shown in Fig. 4.1. This interfacial behaviour is mainly due to spin torques[34]. In a more general calculation, these effects should also be taken into account.

Our setup only applies for media in which our assumptions do justice to the materials used. There are materials for which these simplifications do not apply. A medium with a pyrochlore structure would lead to band structures in the medium, possibly leading to a different outcome. The observed (thermally driven) magnon Hall effect was measured using such a medium[13]. Also, a setup that accounts for dipole-dipole interactions may lead to different results. Furthermore, the use of a lattice model to describe the bulk rather than a continuous medium could lead to a prediction of the transverse current, through band structures and anomalous velocities.

The method of calculation itself, in general, can have fruitful results when examining spin currents, as can be seen from our calculation of the longitudinal spin current. We see that DMI does manifest itself in the longitudinal spin current.

Looking forward, it seems a logical step to redefine this setup so that it would apply to different materials, such as pyrochlore structures. Interfacial DMI effects and dipole-dipole interactions could be taken into account, which may lead to the prediction of a nonzero transverse spin current.

Acknowledgements

I would like to thank my supervisors Rembert, Scott and Camilo for all the time, effort and guidance during the last year. The level of investment shown in my work has exceeded my expectations. I really enjoyed the working on the project, which is the culmination of seven years of studying physics.

My understanding of the matter covered in chapter 2 has significantly improved due to the help of Camilo, aiding me in the development of a Mathematica model that I used to compute the dispersion relations. The Mathematica model supplied by Rick Keesman was also very helpful in the animations of 2D lattices. For chapter 3, the notes of Scott, as well as those of Yaroslav Tserkovnyak proved extremely useful.

Bibliography

[1] Wolf, S. A., et al. "Spintronics: a spin-based electronics vision for the future." Science 294.5546 (2001): 1488-1495.

[2] McCray, W. Patrick. "How spintronics went from the lab to the iPod." Nature Nanotechnology 4, 2 - 4 (2009)

[3] "The Nobel Prize in Physics 2007: Information for the Public" The Royal Swedish Academy of Sciences, (2007).

[4] Kono, Junichiro. "Spintronics: Coherent terahertz control." Nature Photonics 5.1 (2011): 5-6.

[5] Chumak, A. V., et al. "Magnon spintronics." Nature Physics 11.6 (2015): 453-461.

[6] Pulizzi, F. "Spintronics." Nature Materials 11, 367 (2012)

[7] Sinova, J., et al. "New moves of the spintronics tango." Nature Materials 11, 368–371 (2012)

[8] Liu, Luqiao, et al. "Spin-torque ferromagnetic resonance induced by the spin Hall effect." Physical review letters 106.3 (2011): 036601.

[9] https://en.wikipedia.org/wiki/Spin_Hall_effect

[10] Uchida, K., et al. "Observation of the spin Seebeck effect." Nature 455.7214 (2008): 778-781.

[11] Hall, E. H. "On a New Action of the Magnet on Electric Currents." American Journal of Mathematics, vol. 2, no. 3, 1879, pp. 287–292.

[12] Kajiwara, Y., et al. "Transmission of electrical signals by spin-wave interconversion in a magnetic insulator." Nature 464.7286 (2010): 262-266.

[13] Onose, Y., et al. "Observation of the magnon Hall effect." Science 329.5989 (2010): 297-299.

[14] Cornelissen, L. J., et al. "Long-distance transport of magnon spin information in a magnetic insulator at room temperature." Nature Physics 11.12 (2015): 1022-1026.

[15] https://www.slideshare.net/koukiNakata/josephson-and-persistent/-spin-currents-in-boseeinstein-condensates-of-magnons, slide 31, on 22-6-2017

[16] Adachi, Hiroto, et al. "Theory of the spin Seebeck effect." Reports on Progress in Physics 76.3 (2013): 036501.

[17] Matsumoto, Ryo, and Shuichi Murakami. "Rotational motion of magnons and the thermal Hall effect." Physical Review B 84.18 (2011): 184406.

[18] Meijs, R., "The electrically driven magnon Hall effect in YIG/Pt heterostructures", Bachelor Thesis, Universiteit Utrecht, 2015.

[19] Ganzhorn, Kathrin, et al. "Magnon-based logic in a multi-terminal YIG/Pt nanostructure." Applied Physics Letters 109.2 (2016): 022405.

[20] Stancil, Daniel D., and Anil Prabhakar. Spin waves. Luxembourg: Springer, 2009.

[21] https://www.uni-muenster.de/Physik.AP/Demokritov/en/Forschen/Forschungsschwerpunkte/mBECwasw.html On 10-6-2017

[22] Arai, H., et al. "Spin-wave excitations induced by spin current through a magnetic point contact with a confined domain wall." Applied Physics Letters 101 (9), 092405

[23] http://muonray.blogspot.nl/2013/10/ on 22-6-2017

[24] http://nnspnt.snu.ac.kr/html/research/research.php on 22-6-2017

[25] https://www.uni-muenster.de/Physik.AP/Demokritov/en/Forschen/Forschungsschwerpunkte/mBECwam.html on 22-6-2017

[26] Ulloa Osorio, Camilo Edgardo. "Aspects of antiferromagnetic spintronics." (2016).

[27] Heide, M., G. Bihlmayer, and S. Blügel. "Dzyaloshinskii-Moriya interaction accounting for the orientation of magnetic domains in ultrathin films: Fe/W (110)." Physical Review B 78.14 (2008): 140403.

[28] http://www.nanoscience.de/HTML/research/noncollinear_spins.html on 10-6-2017

[29] Gambardella, Pietro, and Ioan Mihai Miron. "Current-induced spin–orbit torques." Philosophical Transactions of the Royal Society of London A: Mathematical, Physical and Engineering Sciences 369.1948 (2011): 3175-3197.

[30] Brzeźniak, Zdzislaw, Beniamin Goldys, and Terence Jegaraj. "Weak solutions of a stochastic Landau–Lifshitz–Gilbert equation." Applied Mathematics Research eXpress 2013.1 (2012): 1-33.

[31] Romá, Federico, Leticia F. Cugliandolo, and Gustavo S. Lozano. "Numerical integration of the stochastic Landau-Lifshitz-Gilbert equation in generic time-discretization schemes." Physical Review E 90.2 (2014): 023203.

[32] Bode, Matthias, et al. "Chiral magnetic order at surfaces driven by inversion asymmetry." Nature 447.7141 (2007): 190-193.

[33] Kubo, Rep. "The fluctuation-dissipation theorem." Reports on progress in physics 29.1 (1966): 255.

[34] Rohart, S., and A. Thiaville. "Skyrmion confinement in ultrathin film nanostructures in the presence of Dzyaloshinskii-Moriya interaction." Physical Review B 88.18 (2013): 184422.

Appendix A

Calculation of the equation of motion

We start from the stochastic LLG:

$$\partial_t \mathbf{n} = -\mathbf{n} \times \frac{\delta E}{\delta \mathbf{n}} - \mathbf{n} \times \mathbf{h} - \alpha \mathbf{n} \times \hbar \partial_t \mathbf{n}.$$

As we saw in chapter 2, the linear order contribution of DMI vanishes if we orient the external magnetic field along the z-axis. We will therefore consider the field to be oriented along the x-axis, and linearize the above equation using $\mathbf{n} = (1, \delta n_y, \delta n_z)$. First off,

$$\frac{\delta E}{\delta \mathbf{n}} = -A\nabla^2 \begin{pmatrix} 0 \\ \delta n_y \\ \delta n_z \end{pmatrix} + D \begin{pmatrix} \partial_x n_z \\ \partial_y n_z \\ -\partial_y n_y \end{pmatrix} - H \begin{pmatrix} 1 \\ 0 \\ 0 \end{pmatrix},$$

where we have used the values from Eq. 2.1, relabeled $J \to A$ and $B \to H$, where H also includes any anisotropic terms. This leads to

$$\begin{aligned} \hbar \partial_t n_y &= -A\nabla^2 n_z - D\partial_y n_y + H n_z + h_z + \alpha \hbar \partial_t n_z \\ \hbar \partial_t n_z &= A\nabla^2 n_y - D\partial_y n_z - H n_y - h_y - \alpha \hbar \partial_t n_y. \end{aligned}$$

If we define $n \equiv n_y - i n_z$ and $h \equiv h_y - i h_z$ this leads to

$$\hbar \partial_t n = -iA\nabla^2 n - D\partial_y n + ih + i\alpha \partial_t n + iHn,$$

so that

$$\left[(-i - \alpha)\hbar \partial_t + A\nabla^2 + iD\partial_y - H\right] n = h.$$

Fourier transforming n and h in y, z and t leads to

$$\int \frac{d^2\mathbf{q}}{(2\pi)^2} \int d\omega \left[(-1+i\alpha)\hbar\omega + A\partial_x^2 - A|\mathbf{q}|^2 - Dq_y - H\right] n(x,\mathbf{q},\omega) e^{i(q_y y + q_z z - \omega t)}$$
$$= \int \frac{d^2\mathbf{q}}{(2\pi)^2} \int d\omega h(x,\mathbf{q},\omega) e^{i(q_y y + q_z z - \omega t)},$$

or

$$\int \frac{d^2\mathbf{q}}{(2\pi)^2} \int d\omega A(\partial_x^2 - \kappa^2) n(x,\mathbf{q},\omega) e^{i(q_y y + q_z z - \omega t)} = \int \frac{d^2\mathbf{q}}{(2\pi)^2} \int d\omega h(x,\mathbf{q},\omega) e^{i(q_y y + q_z z - \omega t)},$$

where

$$\kappa^2 = |\mathbf{q}|^2 + \frac{H + Dq_y + (1-i\alpha)\hbar\omega}{A},$$

which, for brevity, we will write as

$$\left[(-1+i\alpha)\hbar\omega + A\partial_x^2 - A|\mathbf{q}|^2 - Dq_y - H\right] n = h$$

and

$$A(\partial_x^2 - \kappa^2) n = h,$$

where we will re-introduce the integrals and powers of e if necessary.

Appendix B

Calculation of the boundary conditions

From the definition of the current we know

$$-\nabla \cdot \mathbf{j} = s\partial_t \mathbf{m}.$$

Using the LLG, this leads to

$$\mathbf{j}_s(s=0) = -As \left\langle \mathbf{n} \times \partial_x \mathbf{n} \right\rangle |_{x=0},$$

where any DMI contributions vanish, as we will explain later. In computing the right hand side of the equation above, we perform the integral

$$\int_{0^-}^{0^+} dx - \mathbf{n} \times \mathbf{H}_{eff} - \mathbf{n} \times \mathbf{h} - (1 + \alpha \mathbf{n} \times) \hbar \partial_t \mathbf{n}.$$

The contribution of $\mathbf{H}_{eff}$ vanishes if we perform this integral, whereas, at the boundary, α is represented by $\frac{g^{\uparrow\downarrow}}{4\pi}$, where $g^{\uparrow\downarrow}$ is a mixing constant. Obviously, a spin accumulation $\boldsymbol{\mu}'$ is picked up as well. At $x = 0$, the boundary condition without DMI contribution reads

$$\mathbf{j}_s(x=0) = -As\mathbf{n} \times \partial_x \mathbf{n}|_{x=0} = -\left[\frac{g^{\uparrow\downarrow}}{4\pi} (\mathbf{n} \times (\mathbf{n} \times \boldsymbol{\mu}') + \mathbf{n} \times \hbar \dot{\mathbf{n}}) + \mathbf{n} \times \mathbf{h}'_L \right]_{x=0},$$

whereas at $x = d$, the boundary condition without DMI contribution reads

$$\mathbf{j}_s(x=d) = -As\mathbf{n} \times \partial_x \mathbf{n}|_{x=d} = \left[\frac{g^{\uparrow\downarrow}}{4\pi} (\mathbf{n} \times \hbar \dot{\mathbf{n}}) + \mathbf{n} \times \mathbf{h}'_R \right]_{x=d},$$

where we assume the spin accumulation $\boldsymbol{\mu}' = \mu' \hat{x}$ vanishes at the (x=d)-interface, and $\mathbf{h}'_L, \mathbf{h}'_R$ represent the stochastic terms at the left and right interface, respectively. Furthermore, s is the spin density, and the contribution of the effective field H vanishes at

the boundaries. Calculations tell us that the DMI contribution at the boundary vanishes. To account for DMI, we start from (see Eq. 2.1)

$$\frac{\delta E_{DMI}}{\delta \mathbf{n}} = D \begin{pmatrix} \partial_x n_z \\ \partial_y n_z \\ -(\partial_x n_x + \partial_y n_y) \end{pmatrix}.$$

In the LLG equation, the contribution will look like

$$-\mathbf{n} \times \mathbf{H}_{DMI} = -D \begin{pmatrix} -n_y(\partial_x n_x + \partial_y n_y) - n_z \partial_y n_z \\ n_z \partial_x n_z + n_x(\partial_x n_x + \partial_y n_y) \\ n_x \partial_y n_z - n_y \partial_x n_z \end{pmatrix}.$$

If we want to find the interfacial boundary condition at $x = 0$, we have to solve the integral

$$\int_{0^-}^{0^+} dx - \mathbf{n} \times \mathbf{H}_{DMI},$$

where $0^{\pm}$ denotes $0 \pm \epsilon$, with $\epsilon \to 0$. In this case, we can discard all partial derivatives which are not with respect to x, as they will vanish upon taking this integral. We are thus left with

$$\int_{0^-}^{0^+} dx D \begin{pmatrix} -n_y \partial_x n_x \\ n_z \partial_x n_z \\ -n_y \partial_x n_z \end{pmatrix}.$$

We see that the first and third coordinate are impossible to integrate this way. We will try a different method of incorporating DMI into the boundary condition. Rather than first computing the boundary condition and then linearizing, we linearize the DMI contribution, and only then incorporate it into the linearized boundary condition without DMI. Linearizing with $\mathbf{n} = (1, \delta n_y, \delta n_z)$, we end up with

$$\int_{0^-}^{0^+} dx D \begin{pmatrix} 0 \\ \partial_y n_y \\ \partial_y n_z \end{pmatrix}.$$

We thus conclude that, at $x = 0$, the DMI contribution vanishes. Analogously, we can say the same for the DMI contribution at $x = d$.

Starting from Eq. 3.5 and linearizing around x, we see that

$$-As\mathbf{n} \times \partial_x \mathbf{n}|_{x=0} = -As\partial_x \begin{pmatrix} 0 \\ -n_z \\ n_y \end{pmatrix} \Bigg|_{x=0},$$

and the right hand side of Eq. 3.5 becomes

$$-\left[\frac{g^{\uparrow\downarrow}}{4\pi}\left\{\mu'\begin{pmatrix}0\\ n_y\\ n_z\end{pmatrix}+\hbar\partial_t\begin{pmatrix}0\\ -n_z\\ n_y\end{pmatrix}\right\}+\begin{pmatrix}0\\ -h'_{L,z}\\ h'_{L,y}\end{pmatrix}\right]_{x=0}.$$

Defining, as before, $n \equiv n_y - in_z$ and $h_L \equiv h'_{L,y} - ih'_{L,z}$ we see

$$-As\partial_x n|_{x=0} = -\left[\frac{g^{\uparrow\downarrow}}{4\pi}\left\{i\mu' n + \hbar\partial_t n\right\} + h\right]_{x=0},$$

so that the boundary condition at $x = 0$ becomes

$$As\partial_x n - \frac{g^{\uparrow\downarrow}}{4\pi}[i\mu' + \hbar\partial_t]n = h.$$

Fourier transforming n and h in t and defining $\psi \equiv n\sqrt{s}$, this becomes

$$\left\{A\partial_x + i\frac{g^{\uparrow\downarrow}}{4\pi s}[\hbar\omega - \mu']\right\}\psi = \frac{h_L}{\sqrt{s}}.$$

Analogously, Eq. 3.6 leads to

$$\left\{A\partial_x - i\frac{g^{\uparrow\downarrow}}{4\pi s}\hbar\omega\right\}\psi = -\frac{h_R}{\sqrt{s}}.$$

Appendix C

Computation of the interfacial transverse current

To compute the interfacial current in the y-direction, we use the formula

$$\left\langle \hat{j}_y^{(I)}(x) \right\rangle = \left\langle \psi^*(x) \frac{\hat{v}_{q,y}}{2} \psi(x) \right\rangle .$$

What follows is an intuitive motivation for this formula. We start from a setup *without* DMI, and look at the *longitudinal* current. As we're looking for a current of spins pointed in the x-direction (the direction of the equilibrium), we see

$$\left\langle \hat{j}_x^{(I)}(x) \right\rangle = -As\hat{x} \cdot \langle \mathbf{n} \times \partial_x \mathbf{n} \rangle .$$

First off,

$$x \cdot \langle \mathbf{n} \times \partial_x \mathbf{n} \rangle = \langle n_y \partial_x n_z - n_z \partial_x n_y \rangle .$$

Defining $n \equiv n_y - i n_z$, we see that

$$\mathrm{Re}\Big[i \partial_x (n) n^* \Big] = \partial_x (n_z) n_y - n_z \partial_x (n_y),$$

so that

$$x \cdot \langle \mathbf{n} \times \partial_x \mathbf{n} \rangle = \mathrm{Im}\Big[- \partial_x (n) n^* \Big].$$

Plugging this into the formula for $\left\langle \hat{j}_x^{(I)}(x) \right\rangle$ above, and setting $\psi = n\sqrt{s}$, we get

$$\left\langle \hat{j}_x^{(I)}(x) \right\rangle = A \mathrm{Im}\Big[\langle \psi^*(x) \partial_x \psi(x) \rangle \Big].$$

If we now want to calculate the transverse current, it is an intuitive step to say

$$\left\langle \hat{j}_y^{(I)}(x) \right\rangle = A\mathrm{Im}\Big[\langle \psi^*(x)\partial_y\psi(x)\rangle \Big],$$

which equals, as we Fourier transformed the y-direction,

$$A\mathrm{Im}\Big[iq_y \langle \psi^*(x)\psi(x)\rangle \Big] = Aq_y \langle \psi^*(x)\psi(x)\rangle .$$

We now make the step to define a *velocity operator* $\hat{v}_{\mathbf{q}} \equiv \frac{\partial(\hbar\omega\mathbf{q})}{\partial\mathbf{q}}$, where $\hbar\omega$ is taken from the dispersion relation from chapter 2. Still working without DMI, we can write

$$\left\langle \hat{j}_y^{(I)}(x) \right\rangle = A \left\langle \psi^*(x)\frac{\hat{v}_{q_y}}{2}\psi(x) \right\rangle .$$

If we now include DMI, the dispersion relation changes (see Eq. 2.3), so that $\hat{v}_{q_y} = 2Aq_y + D$

So that

$$\left\langle \hat{j}_y^{(I)}(x) \right\rangle = (Aq_y + \frac{D}{2}) \langle \psi^*(x)\psi(x)\rangle .$$

We now continue to calculate $\psi(x)$;

$$\begin{aligned}
\psi(x) &= C_1 e^{\kappa x} + C_2 e^{-\kappa x} \\
&= (\mathcal{D}e^{-\kappa d}h_L - \mathcal{B}h_R)\frac{e^{\kappa x}}{\mathbb{D}\sqrt{s}} + (-\mathcal{C}e^{\kappa d}h_L + \mathcal{A}h_R)\frac{e^{-\kappa x}}{\mathbb{D}\sqrt{s}} \\
&= \left(\left[A\kappa + i\frac{g^{\uparrow\downarrow}}{4\pi s}\hbar\omega \right] e^{-\kappa(d-x)} - \left[-A\kappa + i\frac{g^{\uparrow\downarrow}}{4\pi s}\hbar\omega \right] e^{\kappa(d-x)} \right)\frac{h_L}{\mathbb{D}\sqrt{s}} \\
&\quad + \left(- \left[-A\kappa + i\frac{g^{\uparrow\downarrow}}{4\pi s}[\hbar\omega - \mu'] \right] e^{\kappa x} + \left[A\kappa + i\frac{g^{\uparrow\downarrow}}{4\pi s}[\hbar\omega - \mu'] \right] e^{-\kappa x} \right)\frac{h_R}{\mathbb{D}\sqrt{s}} \\
&= \left[A\kappa\cosh[\kappa(d-x)] - i\frac{g^{\uparrow\downarrow}}{4\pi s}\hbar\omega\sinh[\kappa(d-x)] \right]\frac{2h_L}{\mathbb{D}\sqrt{s}} \\
&\quad + \left[A\kappa\cosh[\kappa x] - i\frac{g^{\uparrow\downarrow}}{4\pi s}[\hbar\omega - \mu']\sinh[\kappa x] \right]\frac{2h_R}{\mathbb{D}\sqrt{s}}.
\end{aligned}$$

As $\langle h_L^* h_R\rangle = \langle h_R^* h_L\rangle = 0$, $\langle \psi^*\psi\rangle$ equals

$$\frac{4\langle h_L^* h_L\rangle}{\mathbb{D}^*\mathbb{D}s}\Big[\quad A^2\kappa^*\kappa\cosh[\kappa^*(d-x)]\cosh[\kappa(d-x)]$$

$$
\begin{aligned}
&-iA\kappa^*\frac{g^{\uparrow\downarrow}}{4\pi s}\hbar\omega\cosh[\kappa^*(d-x)]\sinh[\kappa(d-x)]\\
&+iA\kappa\frac{g^{\uparrow\downarrow}}{4\pi s}\hbar\omega\sinh[\kappa^*(d-x)]\cosh[\kappa(d-x)]\\
&+\left(\frac{g^{\uparrow\downarrow}}{4\pi s}\hbar\omega\right)^2\sinh[\kappa^*(d-x)]\sinh[\kappa(d-x)]\Bigg]\\
\frac{4\langle h_R^* h_R\rangle}{\mathbb{D}^*\mathbb{D}s}\Bigg[\;&A^2\kappa^*\kappa\cosh[\kappa^* x]\cosh[\kappa x]\\
&-iA\kappa^*\frac{g^{\uparrow\downarrow}}{4\pi s}[\hbar\omega-\mu']\cosh[\kappa^* x]\sinh[\kappa x]\\
&+iA\kappa\frac{g^{\uparrow\downarrow}}{4\pi s}[\hbar\omega-\mu']\sinh[\kappa^* x]\cosh[\kappa x]\\
&+\left(\frac{g^{\uparrow\downarrow}}{4\pi s}[\hbar\omega-\mu']\right)^2\sinh[\kappa^* x]\sinh[\kappa x]\Bigg].
\end{aligned}
$$

It is at this point that we re-introduce the integrals and powers of e that were previously omitted. Noting that $\langle\psi^*\psi\rangle$ stands for $\langle\psi^*(x,\mathbf{q},\omega)\psi(x,\mathbf{q'},\omega')\rangle$, we now set out to compute

$$
\int\frac{d^2\mathbf{q}}{(2\pi)^2}\int\frac{d^2\mathbf{q}'}{(2\pi)^2}\int\frac{d\omega}{2\pi}\int\frac{d\omega'}{2\pi}\left\langle\psi(x,\mathbf{q},\omega)^*\psi(x,\mathbf{q}',\omega')\right\rangle e^{i[(q_y'-q_y)y+(q_z'-q_z)z-(\omega'-\omega)t]}.
$$

Using Eq. 3.1 with all its δ's we see that this equals

$$
\begin{aligned}
\int\frac{d^2\mathbf{q}}{(2\pi^2)}\int\frac{d\omega}{2\pi}\Bigg(\frac{16\hbar T}{\mathbb{D}^*\mathbb{D}s}\frac{g^{\uparrow\downarrow}}{4\pi}\quad&A^2\kappa^*\kappa\cosh[\kappa^*(d-x)]\cosh[\kappa(d-x)]\\
&-iA\kappa^*\tfrac{g^{\uparrow\downarrow}}{4\pi s}\hbar\omega\cosh[\kappa^*(d-x)]\sinh[\kappa(d-x)]\\
&+iA\kappa\tfrac{g^{\uparrow\downarrow}}{4\pi s}\hbar\omega\sinh[\kappa^*(d-x)]\cosh[\kappa(d-x)]\\
&+\left(\tfrac{g^{\uparrow\downarrow}}{4\pi s}\hbar\omega\right)^2\sinh[\kappa^*(d-x)]\sinh[\kappa(d-x)]\\
&+A^2\kappa^*\kappa\cosh[\kappa^* x]\cosh[\kappa x]\\
&-iA\kappa^*\tfrac{g^{\uparrow\downarrow}}{4\pi s}[\hbar\omega-\mu']\cosh[\kappa^* x]\sinh[\kappa x]\\
&+iA\kappa\tfrac{g^{\uparrow\downarrow}}{4\pi s}[\hbar\omega-\mu']\sinh[\kappa^* x]\cosh[\kappa x]\\
&+\left(\tfrac{g^{\uparrow\downarrow}}{4\pi s}[\hbar\omega-\mu']\right)^2\sinh[\kappa^* x]\sinh[\kappa x]\Bigg).
\end{aligned}
$$

In Appendix F a dimensional analysis of this formula can be found. We further note that D only enters into $\langle\psi^*\psi\rangle$ through κ. We now redefine $q_y\to\tilde{q}_y=q_y+\frac{D}{2A}$ so that

$$\kappa^2 = \tilde{q}_y^2 + q_z^2 - \left(\frac{D}{2A}\right)^2 + \frac{H - (1 + i\alpha)\hbar\omega}{A}.$$

We see that κ is symmetric under $\tilde{q}_y \to -\tilde{q}_y$. Furthermore, $\int dq_y = \int d\tilde{q}_y$, so that $\langle \psi^* \psi \rangle$ is symmetric under this transformation as well.

Finally, the current $\left\langle j_y^{(I)} \right\rangle$ reads

$$(Aq_y + \frac{D}{2}) \langle \psi^* \psi \rangle = A\tilde{q}_y \langle \psi^* \psi \rangle .$$

Here, of course, both sides have to be integrated over $\tilde{q}_y$. As $\tilde{q}_y$ is antisymmetric under $\tilde{q}_y \to -\tilde{q}_y$ we conclude that, upon integrating over $\tilde{q}_y$, $\left\langle j_y^{(I)} \right\rangle$ vanishes.

Appendix D

Computation of ψ_B

To find ψ_B, we make use of the equation of motion (Eq. 3.3), the fluctutation dissipation theorem (Eq. 3.1) and the bulk boundary conditions, which are similar to the interface boundary conditions (Eq. 3.7 and Eq. 3.8) but with $h_L = h_R = 0$.

Equation of motion:

$$A(\partial_x^2 - \kappa^2)\psi(x,t) = h(x,t)\sqrt{s},$$

where

$$\kappa^2 = |\mathbf{q}|^2 + \frac{H + Dq_y + (1 - i\alpha)\hbar\omega}{A}.$$

Fluctuation dissipation theorem:

$$\left\langle h^*(z,\mathbf{q},\omega)h(y,\mathbf{q}',\omega')\right\rangle = 4(2\pi)^3\alpha\frac{\hbar}{s}T\delta(z-y)\delta(\mathbf{q}-\mathbf{q}')\delta(\omega-\omega').$$

Boundary conditions:

$$\left\{A\partial_x + i\frac{g^{\uparrow\downarrow}}{4\pi s}[\hbar\omega - \mu']\right\}\psi = 0 \text{ at } x = 0,$$

$$\left\{A\partial_x - i\frac{g^{\uparrow\downarrow}}{4\pi s}\hbar\omega\right\}\psi = 0 \text{ at } x = d.$$

Furthermore, we make use of

$$\psi(x) = \int_0^d dy G(x,y)\psi(y) = \int_0^d dy G(x,y)\frac{\sqrt{s}}{A}h(y),$$

where the second equality is due to the equation of motion and where

$$(\partial_x^2 - \kappa^2)G(x,y) = \delta(x-y).$$

Integrating this as follows

$$\int_{y-\epsilon}^{y+\epsilon} dx(\partial_x^2 - \kappa^2)G(x,y) = \int_{y-\epsilon}^{y+\epsilon} dx\delta(x-y) = 1,$$

with $\epsilon \to 0$, we can conclude

$$(\partial_x G^> - \partial_x G^<)|_{x=y} = 1.$$

Defining $G^<(x,y)$ as the Green's function for $x \leq y$ and $G^>(x,y)$ as the Green's function for $x \geq y$, we write as an Ansatz:

$$G(x,y) = \begin{cases} G^<(x,y) = ae^{\kappa x} + be^{-\kappa x} & \text{for } x < y \\ G^>(x,y) = \tilde{a}e^{\kappa x} + \tilde{b}e^{-\kappa x} & \text{for } x > y, \end{cases}$$

where, of course,

$$G^<(x=y) = G^>(x=y).$$

At $x = 0$, we use $G^<$, which leads to

$$\left\{ A\partial_x + i\frac{g^{\uparrow\downarrow}}{4\pi s}[\hbar\omega - \mu'] \right\} G^<(x,y) = 0,$$

so that

$$\begin{aligned} 0 &= A\kappa(a-b) + i\frac{g^{\uparrow\downarrow}}{4\pi s}[\hbar\omega - \mu'](a+b) \\ &= a\left[A\kappa + i\frac{g^{\uparrow\downarrow}}{4\pi s}[\hbar\omega - \mu']\right] + b\left[-A\kappa + i\frac{g^{\uparrow\downarrow}}{4\pi s}[\hbar\omega - \mu']\right], \end{aligned}$$

so

$$a = \sigma b,$$

where

$$\sigma \equiv \frac{A\kappa - i\frac{g^{\uparrow\downarrow}}{4\pi s}[\hbar\omega - \mu']}{A\kappa + i\frac{g^{\uparrow\downarrow}}{4\pi s}[\hbar\omega - \mu']} = -\frac{\mathcal{B}}{\mathcal{A}}.$$

At $x = d$, we use $G^{>}$, which leads to

$$\left\{ A\partial_x - i\frac{g^{\uparrow\downarrow}}{4\pi s}\hbar\omega \right\} G^{>}(x,y) = 0,$$

so that

$$\begin{aligned} 0 &= A\kappa(\tilde{a}e^{\kappa d} - \tilde{b}e^{-\kappa d}) - i\frac{g^{\uparrow\downarrow}}{4\pi s}\hbar\omega(\tilde{a}e^{\kappa d} + \tilde{b}e^{-\kappa d}) \\ &= \tilde{a}\left[A\kappa - i\frac{g^{\uparrow\downarrow}}{4\pi s}\hbar\omega\right]e^{\kappa d} + \tilde{b}\left[-A\kappa - i\frac{g^{\uparrow\downarrow}}{4\pi s}\hbar\omega\tilde{b}\right]e^{-\kappa d}, \end{aligned}$$

so

$$\tilde{a} = \tilde{\sigma}^{-1}\tilde{b}e^{-2\kappa d},$$

where

$$\tilde{\sigma}^{-1} \equiv \frac{A\kappa + i\frac{g^{\uparrow\downarrow}}{4\pi s}\hbar\omega}{A\kappa - i\frac{g^{\uparrow\downarrow}}{4\pi s}\hbar\omega} = -\frac{\mathcal{D}}{\mathcal{C}}.$$

From Eq. 3.11, we see

$$ae^{\kappa y} + be^{-\kappa y} = \tilde{a}e^{\kappa y} + \tilde{b}e^{-\kappa y}.$$

Plugging in our values for a and $\tilde{a}$ leads to

$$\left(\sigma e^{\kappa y} + e^{-\kappa y}\right) b = \left(\tilde{\sigma}^{-1}e^{-2\kappa d}e^{\kappa y} + e^{-\kappa y}\right)\tilde{b},$$

so that

$$b = \left(\frac{\tilde{\sigma}^{-1}e^{-2\kappa d}e^{\kappa y} + e^{-\kappa y}}{\sigma e^{\kappa y} + e^{-\kappa y}}\right)\tilde{b}.$$

From Eq. 3.10 we see

$$\begin{aligned} 1 &= (\tilde{a} - a)\kappa e^{\kappa y} - (\tilde{b} - b)\kappa e^{-\kappa y} \\ &= (\tilde{\sigma}^{-1}\tilde{b}e^{-2\kappa d} - \sigma b)\kappa e^{\kappa y} - (\tilde{b} - b)\kappa e^{-\kappa y} \\ &= \left[\tilde{\sigma}^{-1}e^{-2\kappa d}\kappa e^{\kappa y} - \kappa e^{-\kappa y}\right]\tilde{b} + \left[-\sigma\kappa e^{\kappa y} + \kappa e^{-\kappa y}\right] b \end{aligned}$$

$$
\begin{aligned}
&= \left\{ \left[\tilde{\sigma}^{-1}e^{-2\kappa d}e^{\kappa y} - e^{-\kappa y}\right] + \left[-\sigma e^{\kappa y} + e^{-\kappa y}\right] \left(\frac{\tilde{\sigma}^{-1}e^{-2\kappa d}e^{\kappa y} + e^{-\kappa y}}{\sigma e^{\kappa y} + e^{-\kappa y}} \right) \right\} \kappa\tilde{b} \\
&= \frac{\kappa\tilde{b}}{\sigma e^{\kappa y} + e^{-\kappa y}} \left\{ \left[\tilde{\sigma}^{-1}e^{-2\kappa d}e^{\kappa y} - e^{-\kappa y}\right] \left[\sigma e^{\kappa y} + e^{-\kappa y}\right] \right. \\
&\quad \left. + \left[-\sigma e^{\kappa y} + e^{-\kappa y}\right] \left[\tilde{\sigma}^{-1}e^{-2\kappa d}e^{\kappa y} + e^{-\kappa y}\right] \right\} \\
&= \frac{2\kappa\tilde{b}[\tilde{\sigma}^{-1}e^{-2\kappa d} - \sigma]}{\sigma e^{\kappa y} + e^{-\kappa y}},
\end{aligned}
$$

so

$$
\tilde{b} = \frac{1}{2\kappa} \left(\frac{\sigma e^{\kappa y} + e^{-\kappa y}}{\tilde{\sigma}^{-1}e^{-2\kappa d} - \sigma} \right),
$$

so

$$
\begin{aligned}
b &= \left(\frac{\tilde{\sigma}^{-1}e^{-2\kappa d}e^{\kappa y} + e^{-\kappa y}}{\sigma e^{\kappa y} + e^{-\kappa y}} \right) \frac{1}{2\kappa} \left(\frac{\sigma e^{\kappa y} + e^{-\kappa y}}{\tilde{\sigma}^{-1}e^{-2\kappa d} - \sigma} \right) \\
&= \frac{1}{2\kappa} \left(\frac{\tilde{\sigma}^{-1}e^{-2\kappa d}e^{\kappa y} + e^{-\kappa y}}{\tilde{\sigma}^{-1}e^{-2\kappa d} - \sigma} \right),
\end{aligned}
$$

so

$$
a = \frac{\sigma}{2\kappa} \left(\frac{\tilde{\sigma}^{-1}e^{-2\kappa d}e^{\kappa y} + e^{-\kappa y}}{\tilde{\sigma}^{-1}e^{-2\kappa d} - \sigma} \right),
$$

so

$$
\tilde{a} = \frac{\tilde{\sigma}^{-1}e^{-2\kappa d}}{2\kappa} \left(\frac{\sigma e^{\kappa y} + e^{-\kappa y}}{\tilde{\sigma}^{-1}e^{-2\kappa d} - \sigma} \right).
$$

Appendix E

Computation of the transverse bulk current

We use the formula

$$j_y^{(B)} = (Aq_y + \frac{D}{2}) \langle \psi^*(x)\psi(x) \rangle .$$

We set out to compute $\langle \psi^*(x)\psi(x) \rangle$. We know

$$\psi(x) = \int_0^d dy G(x,y)\psi(y) = \int_0^d dy G(x,y)\frac{\sqrt{s}}{A}h(y),$$

which leads to

$$\langle \psi^*(x)\psi(x) \rangle = \left\langle \left[\int_0^d dz G(x,z)\frac{\sqrt{s}}{A}h(z) \right]^* \left[\int_0^d dy G(x,y)\frac{\sqrt{s}}{A}h(y) \right] \right\rangle .$$

We note that if we were to write out all the integrals and powers of e, the left hand side will have integrals over $\mathbf{q}, \omega$. On the right hand side, the conjugated part will have integrals over $\mathbf{q'}, \omega'$, and the non-conjugated part over $\mathbf{q}, \omega$. Using the Ansatz

$$G(x,y) = \begin{cases} G^<(x,y) = ae^{\kappa x} + be^{-\kappa x} & \text{for } x < y \\ G^>(x,y) = \tilde{a}e^{\kappa x} + \tilde{b}e^{-\kappa x} & \text{for } x > y \end{cases}$$

leads to

$$\begin{aligned} \langle \psi^*(x)\psi(x) \rangle &= \left(\int_0^x dz G^>(x,z)\frac{\sqrt{s}}{A}h(z) + \int_x^d dz G^<(x,z)\frac{\sqrt{s}}{A}h(z) \right)^* \\ &\quad \times \left(\int_0^x dy G^>(x,y)\frac{\sqrt{s}}{A}h(y) + \int_x^d dy G^<(x,y)\frac{\sqrt{s}}{A}h(y) \right) \end{aligned}$$

$$= \left(\int_0^x dz \int_0^x dy [G^>(x,z)]^* G^>(x,y) \frac{s}{A^2} + \int_x^d dz \int_x^d dy [G^<(x,z)]^* G^<(x,y) \frac{s}{A^2} \right) \langle h^*(z) h(y) \rangle .$$

We use Eq. 3.1, which leads to

$$\begin{aligned}
& \underbrace{\int \frac{d^2\mathbf{q}}{(2\pi)^2} \int \frac{d\omega}{2\pi} 4\alpha \frac{\hbar}{A^2} T}_{\Theta} \left(\int_0^x dy [G^>(x,y)]^* G^>(x,y) + \int_x^d dy [G^<(x,y)]^* G^<(x,y) \right) \\
= \; & \Theta \left(\int_0^x dy \left[\tilde{a} e^{\kappa x} + \tilde{b} e^{-\kappa x} \right]^* \left[\tilde{a} e^{\kappa x} + \tilde{b} e^{-\kappa x} \right] + \int_x^d dy \left[a e^{\kappa x} + b e^{-\kappa x} \right]^* \left[a e^{\kappa x} + b e^{-\kappa x} \right] \right) \\
= \; & \Theta \left(\int_0^x dy \left[\tilde{\sigma}^{-1} e^{-2\kappa d} e^{\kappa x} + e^{-\kappa x} \right]^* \tilde{b}^* \tilde{b} \left[\tilde{\sigma}^{-1} e^{-2\kappa d} e^{\kappa x} + e^{-\kappa x} \right] \right. \\
& \left. + \int_x^d dy \left[\sigma e^{\kappa x} + e^{-\kappa x} \right]^* b^* b \left[\sigma e^{\kappa x} + e^{-\kappa x} \right] \right) \\
= \; & \Theta \left(\int_0^x dy e^{-(\kappa+\kappa^*)x} \left[\tilde{\sigma}^{-1} e^{-2\kappa(d-x)} + 1 \right]^* \tilde{b}^* \tilde{b} \left[\tilde{\sigma}^{-1} e^{-2\kappa(d-x)} + 1 \right] \right. \\
& \left. + \int_x^d dy e^{-(\kappa+\kappa^*)x} \left[\sigma e^{2\kappa x} + 1 \right]^* b^* b \left[\sigma e^{2\kappa x} + 1 \right] \right) \\
= \; & \Theta e^{-(\kappa+\kappa^*)x} \left(\int_0^x dy \left\{ \frac{1}{4\kappa^* \kappa} \left(\frac{\sigma e^{\kappa y} + e^{-\kappa y}}{\tilde{\sigma}^{-1} e^{-2\kappa d} - \sigma} \right)^* \left(\frac{\sigma e^{\kappa y} + e^{-\kappa y}}{\tilde{\sigma}^{-1} e^{-2\kappa d} - \sigma} \right) \right. \right. \\
& \left. \left. \times \underbrace{\left[\tilde{\sigma}^{-1} e^{-2\kappa(d-x)} + 1 \right]^* \left[\tilde{\sigma}^{-1} e^{-2\kappa(d-x)} + 1 \right]}_{\eta_1} \right\} \right. \\
& \left. + \int_x^d dy \left\{ \frac{1}{4\kappa^* \kappa} \left(\frac{\tilde{\sigma}^{-1} e^{-2\kappa d} e^{\kappa y} + e^{-\kappa y}}{\tilde{\sigma}^{-1} e^{-2\kappa d} - \sigma} \right)^* \left(\frac{\tilde{\sigma}^{-1} e^{-2\kappa d} e^{\kappa y} + e^{-\kappa y}}{\tilde{\sigma}^{-1} e^{-2\kappa d} - \sigma} \right) \right. \right. \\
& \left. \left. \times \underbrace{\left[\sigma e^{2\kappa x} + 1 \right]^* \left[\sigma e^{2\kappa x} + 1 \right]}_{\eta_2} \right\} \right).
\end{aligned}$$

In order to compare $\left\langle j_y^{(B)} \right\rangle$ to $\left\langle j_y^{(I)} \right\rangle$ we will write $\left\langle j_y^{(B)} \right\rangle$ with $\mathbb{D}^*\mathbb{D}$ in the denominator as well.

$$\tilde{\sigma}^{-1} e^{-2\kappa d} - \sigma = -\frac{\mathcal{D}}{\mathcal{C}} e^{-2\kappa d} + \frac{\mathcal{B}}{\mathcal{A}} = -e^{-\kappa d} \frac{\mathcal{D}\mathcal{A} e^{-\kappa d} - \mathcal{B}\mathcal{C} e^{\kappa d}}{\mathcal{A}\mathcal{C}} = -e^{-\kappa d} \frac{\mathbb{D}}{\mathcal{A}\mathcal{C}},$$

so that $\left\langle j_y^{(B)} \right\rangle$ reads

$$
\begin{aligned}
& \underbrace{\frac{\Theta e^{(\kappa+\kappa^*)(d-x)}}{4\kappa^*\kappa}\frac{\mathcal{A}^*\mathcal{A}\mathcal{C}^*\mathcal{C}}{\mathbb{D}^*\mathbb{D}}}_{\Phi}\Bigg(\eta_1\int_0^x dy[\sigma e^{\kappa y}+e^{-\kappa y}]^*[\sigma e^{\kappa y}+e^{-\kappa y}] \\
& +\eta_2\int_x^d dy[\tilde{\sigma}^{-1}e^{-2\kappa d}e^{\kappa y}+e^{-\kappa y}]^*[\tilde{\sigma}^{-1}e^{-2\kappa d}e^{\kappa y}+e^{-\kappa y}]\Bigg) \\
= \;& \Phi\Bigg(\eta_1\int_0^x dy\Big\{\sigma^*\sigma e^{(\kappa+\kappa^*)y}+\sigma^* e^{-(\kappa-\kappa^*)y}+\sigma e^{(\kappa-\kappa^*)y}+e^{-(\kappa+\kappa^*)y}\Big\} \\
& +\underbrace{\eta_2 e^{-(\kappa+\kappa^*)d}}_{\tilde{\eta}_2}\int_x^d dy[\tilde{\sigma}^{-1}e^{-\kappa(d-y)}+e^{\kappa(d-y)}]^*[\tilde{\sigma}^{-1}e^{-\kappa(d-y)}+e^{\kappa(d-y)}]\Bigg) \\
= \;& \Phi\Bigg(\eta_1\int_0^x dy\Big\{\sigma^*\sigma e^{(\kappa+\kappa^*)y}+\sigma^* e^{-(\kappa-\kappa^*)y}+\sigma e^{(\kappa-\kappa^*)y}+e^{-(\kappa+\kappa^*)y}\Big\} \\
& +\tilde{\eta}_2\int_x^d dy\Big\{[\tilde{\sigma}^{-1}]^*\tilde{\sigma}^{-1}e^{-(\kappa+\kappa^*)(d-y)}+[\tilde{\sigma}^{-1}]^*e^{(\kappa-\kappa^*)(d-y)} \\
& +\tilde{\sigma}^{-1}e^{-(\kappa-\kappa^*)(d-y)}+e^{(\kappa+\kappa^*)(d-y)}\Big\}\Bigg) \\
= \;& \Phi\Bigg(\eta_1\left[\frac{\sigma^*\sigma e^{(\kappa+\kappa^*)y}}{\kappa+\kappa^*}-\frac{\sigma^* e^{-(\kappa-\kappa^*)y}}{\kappa-\kappa^*}+\frac{\sigma e^{(\kappa-\kappa^*)y}}{\kappa-\kappa^*}-\frac{e^{-(\kappa+\kappa^*)y}}{\kappa+\kappa^*}\right]_{y=0}^{y=x} \\
& +\tilde{\eta}_2\left[\frac{[\tilde{\sigma}^{-1}]^*\tilde{\sigma}^{-1}e^{-(\kappa+\kappa^*)(d-y)}}{\kappa+\kappa^*}-\frac{[\tilde{\sigma}^{-1}]^*e^{(\kappa-\kappa^*)(d-y)}}{\kappa-\kappa^*}\right. \\
& \left.+\frac{\tilde{\sigma}^{-1}e^{-(\kappa-\kappa^*)(d-y)}}{\kappa-\kappa^*}-\frac{e^{(\kappa+\kappa^*)(d-y)}}{\kappa+\kappa^*}\right]_{y=x}^{y=d}\Bigg) \\
= \;& \Phi\Bigg(\eta_1\left\{\frac{\sigma^*\sigma[e^{(\kappa+\kappa^*)x}-1]}{\kappa+\kappa^*}-\frac{\sigma^*[e^{-(\kappa-\kappa^*)x}-1]}{\kappa-\kappa^*}+\frac{\sigma[e^{(\kappa-\kappa^*)x}-1]}{\kappa-\kappa^*}-\frac{e^{-(\kappa+\kappa^*)x}-1}{\kappa+\kappa^*}\right\} \\
& +\tilde{\eta}_2\left\{\frac{[\tilde{\sigma}^{-1}]^*\tilde{\sigma}^{-1}[1-e^{-(\kappa+\kappa^*)(d-x)}]}{\kappa+\kappa^*}-\frac{[\tilde{\sigma}^{-1}]^*[1-e^{(\kappa-\kappa^*)(d-x)}]}{\kappa-\kappa^*}\right. \\
& \left.+\frac{\tilde{\sigma}^{-1}[1-e^{-(\kappa-\kappa^*)(d-x)}]}{\kappa-\kappa^*}-\frac{1-e^{(\kappa+\kappa^*)(d-x)}}{\kappa+\kappa^*}\right\}\Bigg).
\end{aligned}
$$

We use $\sigma=-\frac{\mathcal{B}}{\mathcal{A}}$ and $\tilde{\sigma}^{-1}=-\frac{\mathcal{D}}{\mathcal{C}}$ to see that this equals

$$
\begin{aligned}
&\Phi\Bigg(\eta_1\Bigg\{\frac{\mathcal{B}^*\mathcal{B}}{\mathcal{A}^*\mathcal{A}}\frac{e^{(\kappa+\kappa^*)x}-1}{\kappa+\kappa^*}+\frac{\mathcal{B}^*}{\mathcal{A}^*}\frac{e^{-(\kappa-\kappa^*)x}-1}{\kappa-\kappa^*}-\frac{\mathcal{B}}{\mathcal{A}}\frac{e^{(\kappa-\kappa^*)x}-1}{\kappa-\kappa^*}-\frac{e^{-(\kappa+\kappa^*)x}-1}{\kappa+\kappa^*}\Bigg\}\\
&+\tilde{\eta}_2\Bigg\{\frac{\mathcal{D}^*\mathcal{D}}{\mathcal{C}^*\mathcal{C}}\frac{1-e^{-(\kappa+\kappa^*)(d-x)}}{\kappa+\kappa^*}+\frac{\mathcal{D}^*}{\mathcal{C}^*}\frac{1-e^{(\kappa-\kappa^*)(d-x)}}{\kappa-\kappa^*}\\
&-\frac{\mathcal{D}}{\mathcal{C}}\frac{\tilde{\sigma}^{-1}[1-e^{-(\kappa-\kappa^*)(d-x)}]}{\kappa-\kappa^*}-\frac{1-e^{(\kappa+\kappa^*)(d-x)}}{\kappa+\kappa^*}\Bigg\}\Bigg)\\
=\;&\Phi\Bigg(\frac{\eta_1}{\mathcal{A}^*\mathcal{A}}\Bigg\{\mathcal{B}^*\mathcal{B}\frac{e^{(\kappa+\kappa^*)x}-1}{\kappa+\kappa^*}+\mathcal{B}^*\mathcal{A}\frac{e^{-(\kappa-\kappa^*)x}-1}{\kappa-\kappa^*}-\mathcal{A}^*\mathcal{B}\frac{e^{(\kappa-\kappa^*)x}-1}{\kappa-\kappa^*}\\
&-\mathcal{A}^*\mathcal{A}\frac{e^{-(\kappa+\kappa^*)x}-1}{\kappa+\kappa^*}\Bigg\}\\
&+\frac{\tilde{\eta}_2}{\mathcal{C}^*\mathcal{C}}\Bigg\{\mathcal{D}^*\mathcal{D}\frac{1-e^{-(\kappa+\kappa^*)(d-x)}}{\kappa+\kappa^*}+\mathcal{D}^*\mathcal{C}\frac{1-e^{(\kappa-\kappa^*)(d-x)}}{\kappa-\kappa^*}\\
&-\mathcal{C}^*\mathcal{D}\frac{\tilde{\sigma}^{-1}[1-e^{-(\kappa-\kappa^*)(d-x)}]}{\kappa-\kappa^*}-\mathcal{C}^*\mathcal{C}\frac{1-e^{(\kappa+\kappa^*)(d-x)}}{\kappa+\kappa^*}\Bigg\}\Bigg)\\
=\;&\underbrace{\frac{\Phi}{(\kappa+\kappa^*)(\kappa-\kappa^*)}}_{\tilde{\Phi}}\Bigg(\frac{\eta_1}{\mathcal{A}^*\mathcal{A}}\Bigg\{\mathcal{B}^*\mathcal{B}[e^{(\kappa+\kappa^*)x}-1][\kappa-\kappa^*]+\mathcal{B}^*\mathcal{A}[e^{-(\kappa-\kappa^*)x}-1][\kappa+\kappa^*]\\
&-\mathcal{A}^*\mathcal{B}[e^{(\kappa-\kappa^*)x}-1][\kappa+\kappa^*]-\mathcal{A}^*\mathcal{A}[e^{-(\kappa+\kappa^*)x}-1][\kappa-\kappa^*]\Bigg\}\\
&+\frac{\tilde{\eta}_2}{\mathcal{C}^*\mathcal{C}}\Bigg\{\mathcal{D}^*\mathcal{D}[1-e^{-(\kappa+\kappa^*)(d-x)}][\kappa-\kappa^*]+\mathcal{D}^*\mathcal{C}[1-e^{(\kappa-\kappa^*)(d-x)}][\kappa+\kappa^*]\\
&-\mathcal{C}^*\mathcal{D}[1-e^{-(\kappa-\kappa^*)(d-x)}][\kappa+\kappa^*]-\mathcal{C}^*\mathcal{C}[1-e^{(\kappa+\kappa^*)(d-x)}][\kappa-\kappa^*]\Bigg\}\Bigg).
\end{aligned}
$$

We introduce the shorthand notations $\chi \equiv i\frac{g^{\uparrow\downarrow}}{4\pi s}[\hbar\omega-\mu']$ and $\xi \equiv i\frac{g^{\uparrow\downarrow}}{4\pi s}\hbar\omega$ and compute

$$
\begin{aligned}
\mathcal{A}^*\mathcal{A} &= A^2\kappa^*\kappa-\chi A\kappa+\chi A\kappa^*-\chi^2\\
\mathcal{A}^*\mathcal{B} &= -A^2\kappa^*\kappa+\chi A\kappa+\chi A\kappa^*-\chi^2\\
\mathcal{B}^*\mathcal{A} &= -A^2\kappa^*\kappa-\chi A\kappa-\chi A\kappa^*-\chi^2\\
\mathcal{B}^*\mathcal{B} &= A^2\kappa^*\kappa+\chi A\kappa-\chi A\kappa^*-\chi^2\\
\mathcal{C}^*\mathcal{C} &= A^2\kappa^*\kappa+\xi A\kappa-\xi A\kappa^*-\xi^2\\
\mathcal{C}^*\mathcal{D} &= -A^2\kappa^*\kappa-\xi A\kappa-\xi A\kappa^*-\xi^2
\end{aligned}
$$

$$
\begin{aligned}
\mathcal{D}^*\mathcal{C} &= -A^2\kappa^*\kappa + \xi A\kappa + \xi A\kappa^* - \xi^2 \\
\mathcal{D}^*\mathcal{D} &= A^2\kappa^*\kappa - \xi A\kappa + \xi A\kappa^* - \xi^2,
\end{aligned}
$$

so that $\langle\psi^*\psi\rangle$ equals

$$
\begin{aligned}
\frac{\tilde{\Phi}\eta_1}{\mathcal{A}^*\mathcal{A}}\Bigg(& A^2\kappa^*\kappa\Big\{ [e^{(\kappa+\kappa^*)x}-1][\kappa-\kappa^*] - [e^{-(\kappa-\kappa^*)x}-1][\kappa+\kappa^*] \\
& \quad + [e^{(\kappa-\kappa^*)x}-1][\kappa+\kappa^*] - [e^{-(\kappa+\kappa^*)x}-1][\kappa-\kappa^*]\Big\} \\
& + \chi A\kappa\Big\{ [e^{(\kappa+\kappa^*)x}-1][\kappa-\kappa^*] - [e^{-(\kappa-\kappa^*)x}-1][\kappa+\kappa^*] \\
& \quad - [e^{(\kappa-\kappa^*)x}-1][\kappa+\kappa^*] + [e^{-(\kappa+\kappa^*)x}-1][\kappa-\kappa^*]\Big\} \\
& + \chi A\kappa^*\Big\{ -[e^{(\kappa+\kappa^*)x}-1][\kappa-\kappa^*] - [e^{-(\kappa-\kappa^*)x}-1][\kappa+\kappa^*] \\
& \quad - [e^{(\kappa-\kappa^*)x}-1][\kappa+\kappa^*] - [e^{-(\kappa+\kappa^*)x}-1][\kappa-\kappa^*]\Big\} \\
& + \chi^2\Big\{ -[e^{(\kappa+\kappa^*)x}-1][\kappa-\kappa^*] - [e^{-(\kappa-\kappa^*)x}-1][\kappa+\kappa^*] \\
& \quad + [e^{(\kappa-\kappa^*)x}-1][\kappa+\kappa^*] + [e^{-(\kappa+\kappa^*)x}-1][\kappa-\kappa^*]\Big\}\Bigg) \\
+\frac{\tilde{\Phi}\tilde{\eta}_2}{\mathcal{C}^*\mathcal{C}}\Bigg(& A^2\kappa^*\kappa\Big\{ [1-e^{-(\kappa+\kappa^*)(d-x)}][\kappa-\kappa^*] - [1-e^{(\kappa-\kappa^*)(d-x)}][\kappa+\kappa^*] \\
& \quad + [1-e^{-(\kappa-\kappa^*)(d-x)}][\kappa+\kappa^*] - [1-e^{(\kappa+\kappa^*)(d-x)}][\kappa-\kappa^*]\Big\} \\
& + \xi A\kappa\Big\{ -[1-e^{-(\kappa+\kappa^*)(d-x)}][\kappa-\kappa^*] + [1-e^{(\kappa-\kappa^*)(d-x)}][\kappa+\kappa^*] \\
& \quad + [1-e^{-(\kappa-\kappa^*)(d-x)}][\kappa+\kappa^*] - [1-e^{(\kappa+\kappa^*)(d-x)}][\kappa-\kappa^*]\Big\} \\
& + \xi A\kappa^*\Big\{ [1-e^{-(\kappa+\kappa^*)(d-x)}][\kappa-\kappa^*] + [1-e^{(\kappa-\kappa^*)(d-x)}][\kappa+\kappa^*] \\
& \quad + [1-e^{-(\kappa-\kappa^*)(d-x)}][\kappa+\kappa^*] + [1-e^{(\kappa+\kappa^*)(d-x)}][\kappa-\kappa^*]\Big\}
\end{aligned}
$$

$$+\xi^2\Bigg\{\quad -[1-e^{-(\kappa+\kappa^*)(d-x)}][\kappa-\kappa^*]-[1-e^{(\kappa-\kappa^*)(d-x)}][\kappa+\kappa^*]$$
$$+[1-e^{-(\kappa-\kappa^*)(d-x)}][\kappa+\kappa^*]+[1-e^{(\kappa+\kappa^*)(d-x)}][\kappa-\kappa^*]\Bigg\},$$

which equals

$$\frac{2\tilde{\Phi}\eta_1}{\mathcal{A}^*\mathcal{A}}\Bigg(\quad A^2\kappa^*\kappa\quad\Bigg\{\sinh[(\kappa+\kappa^*)x][\kappa-\kappa^*]+\sinh[(\kappa-\kappa^*)x][\kappa+\kappa^*]\Bigg\}$$
$$+\chi A\kappa\quad\Bigg\{\Bigg(\cosh[(\kappa+\kappa^*)x]-1\Bigg)[\kappa-\kappa^*]-\Bigg(\cosh[(\kappa-\kappa^*)x]-1\Bigg)[\kappa+\kappa^*]\Bigg\}$$
$$+\chi A\kappa^*\quad\Bigg\{-\Bigg(\cosh[(\kappa+\kappa^*)x]-1\Bigg)[\kappa-\kappa^*]-\Bigg(\cosh[(\kappa-\kappa^*)x]-1\Bigg)[\kappa+\kappa^*]\Bigg\}$$
$$+\chi^2\quad\Bigg\{-\sinh[(\kappa+\kappa^*)x][\kappa-\kappa^*]+\sinh[(\kappa-\kappa^*)x][\kappa+\kappa^*]\Bigg\}\Bigg)$$
$$+\frac{2\tilde{\Phi}\tilde{\eta}_2}{\mathcal{C}^*\mathcal{C}}\Bigg(\quad A^2\kappa^*\kappa\quad\Bigg\{\sinh\left[(\kappa+\kappa^*)(d-x)\right][\kappa-\kappa^*]+\sinh\left[(\kappa-\kappa^*)(d-x)\right][\kappa+\kappa^*]\Bigg\}$$
$$+\xi A\kappa\quad\Bigg\{\Bigg(\cosh\left[(\kappa+\kappa^*)(d-x)\right]-1\Bigg)[\kappa-\kappa^*]$$
$$-\Bigg(\cosh\left[(\kappa-\kappa^*)(d-x)\right]-1\Bigg)[\kappa+\kappa^*]\Bigg\}$$
$$+\xi A\kappa^*\quad\Bigg\{-\Bigg(\cosh\left[(\kappa+\kappa^*)(d-x)\right]-1\Bigg)[\kappa-\kappa^*]$$
$$-\Bigg(\cosh\left[(\kappa-\kappa^*)(d-x)\right]-1\Bigg)[\kappa+\kappa^*]\Bigg\}$$
$$+\xi^2\quad\Bigg\{-\sinh\left[(\kappa+\kappa^*)(d-x)\right][\kappa-\kappa^*]+\sinh\left[(\kappa-\kappa^*)(d-x)\right][\kappa+\kappa^*]\Bigg\}\Bigg),$$

which equals

$$\frac{2\tilde{\Phi}\eta_1}{\mathcal{A}^*\mathcal{A}}\Bigg(\quad A^2\kappa^*\kappa\quad\Bigg\{\kappa\Bigg[\sinh[(\kappa+\kappa^*)x]+\sinh[(\kappa-\kappa^*)x]\Bigg]$$
$$-\kappa^*\Bigg[\sinh[(\kappa+\kappa^*)x]-\sinh[(\kappa-\kappa^*)x]\Bigg]\Bigg\}$$

$$
\begin{aligned}
&+\chi A\kappa \quad \Big\{\kappa\Big[\cosh[(\kappa+\kappa^*)x]-\cosh[(\kappa-\kappa^*)x]\Big]\\
&\qquad -\kappa^*\Big[\cosh[(\kappa+\kappa^*)x]+\cosh[(\kappa-\kappa^*)x]\Big]+2\kappa^*\Big\}\\
&+\chi A\kappa^* \quad \Big\{-\kappa\Big[\cosh[(\kappa+\kappa^*)x]+\cosh[(\kappa-\kappa^*)x]\Big]\\
&\qquad +\kappa^*\Big[\cosh[(\kappa+\kappa^*)x]-\cosh[(\kappa-\kappa^*)x]\Big]+2\kappa\Big\}\\
&+\chi^2 \quad \Big\{-\kappa\Big[\sinh[(\kappa+\kappa^*)x]-\sinh[(\kappa-\kappa^*)x]\Big]\\
&\qquad +\kappa^*\Big[\sinh[(\kappa+\kappa^*)x]+\sinh[(\kappa-\kappa^*)x]\Big]\Big\}\Big)\\
+\frac{2\tilde{\Phi}\tilde{\eta}_2}{\mathcal{C}^*\mathcal{C}}\Big(&A^2\kappa^*\kappa \quad \Big\{\kappa\Big[\sinh[(\kappa+\kappa^*)(d-x)]+\sinh[(\kappa-\kappa^*)(d-x)]\Big]\\
&\qquad -\kappa^*\Big[\sinh[(\kappa+\kappa^*)(d-x)]-\sinh[(\kappa-\kappa^*)(d-x)]\Big]\Big\}\\
&+\xi A\kappa \quad \Big\{\kappa\Big[\cosh[(\kappa+\kappa^*)(d-x)]-\cosh[(\kappa-\kappa^*)(d-x)]\Big]\\
&\qquad -\kappa^*\Big[\cosh[(\kappa+\kappa^*)(d-x)]+\cosh[(\kappa-\kappa^*)(d-x)]\Big]+2\kappa^*\Big\}\\
&+\xi A\kappa^* \quad \Big\{-\kappa\Big[\cosh[(\kappa+\kappa^*)(d-x)]+\cosh[(\kappa-\kappa^*)(d-x)]\Big]\\
&\qquad +\kappa^*\Big[\cosh[(\kappa+\kappa^*)(d-x)]-\cosh[(\kappa-\kappa^*)(d-x)]\Big]+2\kappa\Big\}\\
&+\xi^2 \quad \Big\{-\kappa\Big[\sinh[(\kappa+\kappa^*)(d-x)]-\sinh[(\kappa-\kappa^*)(d-x)]\Big]\\
&\qquad +\kappa^*\Big[\sinh[(\kappa+\kappa^*)(d-x)]+\sinh[(\kappa-\kappa^*)(d-x)]\Big]\Big\}\Big).
\end{aligned}
$$

We use

$$
\begin{aligned}
\sinh[(\kappa+\kappa^*)x]+\sinh[(\kappa-\kappa^*)x] &= 2\sinh[\kappa x]\cosh[\kappa^* x]\\
\sinh[(\kappa+\kappa^*)x]-\sinh[(\kappa-\kappa^*)x] &= 2\cosh[\kappa x]\sinh[\kappa^* x]
\end{aligned}
$$

$$\cosh[(\kappa+\kappa^*)x]-\cosh[(\kappa-\kappa^*)x]=2\sinh[\kappa x]\sinh[\kappa^* x]$$
$$\cosh[(\kappa+\kappa^*)x]+\cosh[(\kappa-\kappa^*)x]=2\cosh[\kappa x]\cosh[\kappa^* x],$$

and see

$$\begin{aligned}
\frac{4\tilde{\Phi}\eta_1}{\mathcal{A}^*\mathcal{A}}\Bigg(\quad & A^2\kappa^*\kappa \quad \left\{\kappa\left[\sinh[\kappa x]\cosh[\kappa^* x]\right]-\kappa^*\left[\cosh[\kappa x]\sinh[\kappa^* x]\right]\right\} \\
& +\chi A\kappa \quad \left\{\kappa\left[\sinh[\kappa x]\sinh[\kappa^* x]\right]-\kappa^*\left[\cosh[\kappa x]\cosh[\kappa^* x]\right]+\kappa^*\right\} \\
& +\chi A\kappa^* \quad \left\{-\kappa\left[\cosh[\kappa x]\cosh[\kappa^* x]\right]+\kappa^*\left[\sinh[\kappa x]\sinh[\kappa^* x]\right]+\kappa\right\} \\
& +\chi^2 \quad \left\{-\kappa\left[\cosh[\kappa x]\sinh[\kappa^* x]\right]+\kappa^*\left[\sinh[\kappa x]\cosh[\kappa^* x]\right]\right\}\Bigg) \\
+\frac{4\tilde{\Phi}\tilde{\eta}_2}{\mathcal{C}^*\mathcal{C}}\Bigg(\quad & A^2\kappa^*\kappa \quad \left\{\kappa\left[\sinh[\kappa(d-x)]\cosh[\kappa^*(d-x)]\right]\right. \\
& \qquad \left.-\kappa^*\left[\cosh[\kappa(d-x)]\sinh[\kappa^*(d-x)]\right]\right\} \\
& +\xi A\kappa \quad \left\{\kappa\left[\sinh[\kappa(d-x)]\sinh[\kappa^*(d-x)]\right]\right. \\
& \qquad \left.-\kappa^*\left[\cosh[\kappa(d-x)]\cosh[\kappa^*(d-x)]\right]+\kappa^*\right\} \\
& +\xi A\kappa^* \quad \left\{-\kappa\left[\cosh[\kappa(d-x)]\cosh[\kappa^*(d-x)]\right]\right. \\
& \qquad \left.+\kappa^*\left[\sinh[\kappa(d-x)]\sinh[\kappa^*(d-x)]\right]+\kappa\right\} \\
& +\xi^2 \quad \left\{-\kappa\left[\cosh[\kappa(d-x)]\sinh[\kappa^*(d-x)]\right]\right. \\
& \qquad \left.+\kappa^*\left[\sinh[\kappa(d-x)]\cosh[\kappa^*(d-x)]\right]\right\}\Bigg).
\end{aligned} \tag{E.1}$$

Before going any further, we have to take a closer look at η_1 and $\tilde{\eta}_2$. We see that

$$\tilde{\sigma}^{-1}e^{-2\kappa(d-x)}+1 \;=\; \frac{-\mathcal{D}e^{-2\kappa(d-x)}+\mathcal{C}}{\mathcal{C}}=\frac{-e^{-\kappa(d-x)}}{\mathcal{C}}\left(\mathcal{D}e^{-\kappa(d-x)}-\mathcal{C}e^{\kappa(d-x)}\right)$$

$$
\begin{aligned}
&= \frac{-e^{-\kappa(d-x)}}{\mathcal{C}}\left[(A\kappa+\xi)\,e^{-\kappa(d-x)}+(A\kappa-\xi)\,e^{\kappa(d-x)}\right]\\
&= \frac{-2e^{-\kappa(d-x)}}{\mathcal{C}}\left[A\kappa\cosh[\kappa(d-x)]-\xi\sinh[\kappa(d-x)]\right],
\end{aligned}
$$

and

$$
\begin{aligned}
\sigma e^{2\kappa x}+1 &= \frac{-\mathcal{B}e^{2\kappa x}+\mathcal{A}}{\mathcal{A}} = \frac{e^{\kappa x}}{\mathcal{A}}\left[-\mathcal{B}e^{\kappa x}+\mathcal{A}e^{-\kappa x}\right]\\
&= \frac{e^{\kappa x}}{\mathcal{A}}\left[(A\kappa-\chi)e^{\kappa x}+(A\kappa+\chi)e^{-\kappa x}\right]\\
&= \frac{2e^{\kappa x}}{\mathcal{A}}\left[A\kappa\cosh[\kappa x]-\chi\sinh[\kappa x]\right],
\end{aligned}
$$

so that

$$
\begin{aligned}
\eta_1 &= \left[\tilde{\sigma}^{-1}e^{-2\kappa(d-x)}+1\right]^*\left[\tilde{\sigma}^{-1}e^{-2\kappa(d-x)}+1\right]\\
&= \frac{4e^{-(\kappa+\kappa^*)(d-x)}}{\mathcal{C}^*\mathcal{C}}\left[A\kappa\cosh[\kappa(d-x)]-\xi\sinh[\kappa(d-x)]\right]^*\\
&\quad\times\left[A\kappa\cosh[\kappa(d-x)]-\xi\sinh[\kappa(d-x)]\right]\\
&= \frac{4e^{-(\kappa+\kappa^*)(d-x)}}{\mathcal{C}^*\mathcal{C}}\Big[A^2\kappa^*\kappa\Big(\cosh[\kappa^*(d-x)]\cosh[\kappa(d-x)]\Big)\\
&\quad-\xi A\kappa^*\Big(\cosh[\kappa^*(d-x)]\sinh[\kappa(d-x)]\Big)+\xi A\kappa\Big(\sinh[\kappa^*(d-x)]\cosh[\kappa(d-x)]\Big)\\
&\quad+\xi^2\Big(\sinh[\kappa^*(d-x)]\sinh[\kappa(d-x)]\Big)\Big]
\end{aligned}
$$

and

$$
\begin{aligned}
\tilde{\eta}_2 &= [\sigma e^{2\kappa x}+1]^*[\sigma e^{2\kappa x}+1]e^{-(\kappa+\kappa^*)d}\\
&= \frac{4e^{-(\kappa+\kappa^*)(d-x)}}{\mathcal{A}^*\mathcal{A}}\left[A\kappa\cosh[\kappa x]-\chi\sinh[\kappa x]\right]^*\left[A\kappa\cosh[\kappa x]-\chi\sinh[\kappa x]\right]\\
&= \frac{4e^{-(\kappa+\kappa^*)(d-x)}}{\mathcal{A}^*\mathcal{A}}\Big[A^2\kappa^*\kappa\Big(\cosh[\kappa^*x]\cosh[\kappa x]\Big)-\chi A\kappa^*\Big(\cosh[\kappa^*x]\sinh[\kappa x]\Big)\\
&\quad+\chi A\kappa\Big(\sinh[\kappa^*x]\cosh[\kappa x]\Big)+\chi^2\Big(\sinh[\kappa^*x]\sinh[\kappa x]\Big)\Big].
\end{aligned}
$$

We now define

$$\Omega \equiv \int \frac{d^2\mathbf{q}}{(2\pi)^2} \int \frac{d\omega}{2\pi} \alpha \frac{\hbar}{A^2} T \frac{32}{\kappa^*\kappa} \frac{1}{\mathbb{D}^*\mathbb{D}} \frac{1}{(\kappa+\kappa^*)(\kappa-\kappa^*)}.$$

Also,

$$(\kappa+\kappa^*)(\kappa-\kappa^*) = \kappa^2 - (\kappa^*)^2 = -\frac{2i\alpha\hbar\omega}{A},$$

so that we can write Ω as

$$\Omega = \int \frac{d^2\mathbf{q}}{(2\pi)^2} \int \frac{d\omega}{2\pi} \frac{16iT}{\omega A\kappa^*\kappa} \frac{1}{\mathbb{D}^*\mathbb{D}}.$$

We also define

$$\begin{aligned}
\tilde{\beta}_1 &\equiv A^2\kappa^*\kappa\Big(\cosh[\kappa^*(d-x)]\cosh[\kappa(d-x)]\Big) \\
&\quad -\xi A\kappa^*\Big(\cosh[\kappa^*(d-x)]\sinh[\kappa(d-x)]\Big) + \xi A\kappa\Big(\sinh[\kappa^*(d-x)]\cosh[\kappa(d-x)]\Big) \\
&\quad +\xi^2\Big(\sinh[\kappa^*(d-x)]\sinh[\kappa(d-x)]\Big) \\
\tilde{\beta}_2 &\equiv A^2\kappa^*\kappa\Big(\cosh[\kappa^*x]\cosh[\kappa x]\Big) - \chi A\kappa^*\Big(\cosh[\kappa^*x]\sinh[\kappa x]\Big) \\
&\quad +\chi A\kappa\Big(\sinh[\kappa^*x]\cosh[\kappa x]\Big) + \chi^2\Big(\sinh[\kappa^*x]\sinh[\kappa x]\Big),
\end{aligned}$$

so that

$$\frac{4\tilde{\Phi}\eta_1}{\mathcal{A}^*\mathcal{A}} = \frac{\Omega}{2}\tilde{\beta}_1 \text{ and } \frac{4\tilde{\Phi}\tilde{\eta}_2}{\mathcal{C}^*\mathcal{C}} = \frac{\Omega}{2}\tilde{\beta}_2.$$

We now want to employ a certain trick, for which we have to rewrite the formula for the current. We first had

$$j_y^{(B)} = (Aq_y + \frac{D}{2}) \langle\psi^*\psi\rangle . \tag{E.2}$$

As the right hand side is real (as it should be), we can also write this as

$$\text{Im}\left[i \times (Aq_y + \frac{D}{2}) \langle\psi^*\psi\rangle\right]. \tag{E.3}$$

We note that $\tilde{\beta}_1^* = \tilde{\beta}_1$ and $\tilde{\beta}_2^* = \tilde{\beta}_2$. If we absorb the "$i$" from the expression above into Ω, letting $\tilde{\Omega} \equiv i\Omega$, we see that $\tilde{\Omega}^* = \tilde{\Omega}$. In our new expression for the current, the only

parts that may be imaginary are contained within the round brackets in Eq. E.1. We know that, for any complex number $\mathbb{W}, \mathrm{Im}\left[\mathbb{W}\right] = \mathrm{Im}\left[-\mathbb{W}^*\right]$. We can use this identity on the imaginary parts of our expression for the current.

For the first part in the round brackets (the part behind η_1) in Eq. E.1 this means

$$
\begin{aligned}
A^2\kappa^*\kappa \quad & \left\{ \kappa \left[\sinh[\kappa x] \cosh[\kappa^* x] \right] \underbrace{+\kappa \left[\cosh[\kappa^* x] \sinh[\kappa x] \right]}_{changes} \right\} \\
+\chi A\kappa \quad & \left\{ \kappa \left[\sinh[\kappa x] \sinh[\kappa^* x] \right] - \kappa^* \left[\cosh[\kappa x] \cosh[\kappa^* x] \right] + \kappa^* \right\} \\
+ \underbrace{\chi A\kappa}_{changes} \quad & \underbrace{\left\{ - \kappa^* \left[\cosh[\kappa x] \cosh[\kappa^* x] \right] + \kappa \left[\sinh[\kappa x] \sinh[\kappa^* x] \right] + \kappa^* \right\}}_{changes} \\
+\chi^2 \quad & \left\{ - \kappa \left[\cosh[\kappa x] \sinh[\kappa^* x] \right] \underbrace{-\kappa \left[\sinh[\kappa^* x] \cosh[\kappa x] \right]}_{changes} \right\},
\end{aligned}
$$

and for the second part in the round brackets (the part behind $\tilde{\eta}_2$) in Eq. E.1 this means

$$
\begin{aligned}
A^2\kappa^*\kappa \quad & \left\{ \kappa \left[\sinh[\kappa(d-x)] \cosh[\kappa^*(d-x)] \right] \underbrace{+\kappa \left[\cosh[\kappa^*(d-x)] \sinh[\kappa(d-x)] \right]}_{changes} \right\} \\
+\xi A\kappa \quad & \left\{ \kappa \left[\sinh[\kappa(d-x)] \sinh[\kappa^*(d-x)] \right] \right. \\
& \left. -\kappa^* \left[\cosh[\kappa(d-x)] \cosh[\kappa^*(d-x)] \right] + \kappa^* \right\} \\
\underbrace{-\xi A\kappa}_{changes} \quad & \underbrace{\left\{ \kappa^* \left[\cosh[\kappa(d-x)] \cosh[\kappa^*(d-x)] \right] \right.}_{changes} \\
& \underbrace{\left. -\kappa \left[\sinh[\kappa(d-x)] \sinh[\kappa^*(d-x)] \right] - \kappa^* \right\}}_{changes} \\
+\xi^2 \quad & \left\{ - \kappa \left[\cosh[\kappa(d-x)] \sinh[\kappa^*(d-x)] \right] \right.
\end{aligned}
$$

$$\underbrace{-\kappa\Big[\sinh[\kappa^*(d-x)]\cosh[\kappa(d-x)]\Big]}_{changes}\Bigg\}.$$

As all the other parts of the expression for the current have no imaginary part, they are unaffected by this operation. The two expressions above equal

$$\begin{aligned}
&2A^2\kappa^*\kappa \quad \Bigg\{\kappa\Big[\sinh[\kappa x]\cosh[\kappa^* x]\Big]\Bigg\}\\
&+2\chi A\kappa \quad \Bigg\{\kappa\Big[\sinh[\kappa x]\sinh[\kappa^* x]\Big]-\kappa^*\Big[\cosh[\kappa x]\cosh[\kappa^* x]\Big]+\kappa^*\Bigg\}\\
&+2\chi^2 \quad \Bigg\{-\kappa\Big[\cosh[\kappa x]\sinh[\kappa^* x]\Big]\Bigg\}
\end{aligned}$$

and

$$\begin{aligned}
&2A^2\kappa^*\kappa \quad \Bigg\{\kappa\Big[\sinh[\kappa(d-x)]\cosh[\kappa^*(d-x)]\Big]\Bigg\}\\
&+2\xi A\kappa \quad \Bigg\{\kappa\Big[\sinh[\kappa(d-x)]\sinh[\kappa^*(d-x)]\Big]\\
&\qquad\qquad -\kappa^*\Big[\cosh[\kappa(d-x)]\cosh[\kappa^*(d-x)]\Big]+\kappa^*\Bigg\}\\
&+2\xi^2 \quad \Bigg\{-\kappa\Big[\cosh[\kappa(d-x)]\sinh[\kappa^*(d-x)]\Big]\Bigg\},
\end{aligned}$$

so that $j_y^{(B)}$ equals

$$\begin{aligned}
\mathrm{Im}\Bigg[(Aq_y+\frac{D}{2})\tilde{\Omega}\tilde{\beta}_1\Bigg(\quad & A^2\kappa^*\kappa \quad \Bigg\{\kappa\Big[\sinh[\kappa x]\cosh[\kappa^* x]\Big]\Bigg\}\\
&+\chi A\kappa \quad \Bigg\{\kappa\Big[\sinh[\kappa x]\sinh[\kappa^* x]\Big]-\kappa^*\Big[\cosh[\kappa x]\cosh[\kappa^* x]\Big]+\kappa^*\Bigg\}\\
&+\chi^2 \quad \Bigg\{-\kappa\Big[\cosh[\kappa x]\sinh[\kappa^* x]\Big]\Bigg\}\Bigg)\\
+(Aq_y+\frac{D}{2})\tilde{\Omega}\tilde{\beta}_2\Bigg(\quad & A^2\kappa^*\kappa \quad \Bigg\{\kappa\Big[\sinh[\kappa(d-x)]\cosh[\kappa^*(d-x)]\Big]\Bigg\}
\end{aligned}$$

$$
\begin{aligned}
+\xi A\kappa \quad & \Bigg\{ \kappa \Big[\sinh[\kappa(d-x)] \sinh[\kappa^*(d-x)] \Big] \\
& \quad -\kappa^* \Big[\cosh[\kappa(d-x)] \cosh[\kappa^*(d-x)] \Big] + \kappa^* \Bigg\} \\
+\xi^2 \quad & \Bigg\{ -\kappa \Big[\cosh[\kappa(d-x)] \sinh[\kappa^*(d-x)] \Big] \Bigg\} \Bigg) \Bigg].
\end{aligned}
$$

A dimensional analysis of this formula can be found in Appendix F.

Appendix F

Dimensional analysis of the currents

From Eq. 3.4 we see $[\kappa] = \frac{1}{length}$, $[A] = (energy)(length)^2$ (as $[\hbar\omega] = (energy)$, and $[\alpha] = 1$.

From Eq. 3.5, where we want to have $[j] = \frac{energy}{(length)^2}$,

Knowing that $[A] = (energy)(length)^2$, we see that $[s] = (length)^{-3}$.

Also, as $[\hbar] = (energy)(time)$ we see $[g^{\uparrow\downarrow}] = \frac{1}{(length)^2}$.

Hence $[\mu'] = energy$,

And $[h(\mathbf{x}, t)] = \frac{(energy)}{(length)^2}$.

These dimensions lead to $\mathcal{A} = (energy)(length)$ and $\mathbb{D} = (energy)^2(length)^2$.

We can use these values in the FDT (Eq. 3.1) to obtain $[T] = (energy)$.

F.1 Interfacial current

Looking at the final formula for $\langle\psi^*\psi\rangle$ from section 3.2, writing $length \equiv l, energy \equiv E, time \equiv t$, we see that its dimension is

$$\begin{aligned} & \left[\int \frac{d^2\mathbf{q}}{(2\pi^2)} \int \frac{d\omega}{2\pi} \frac{16\hbar T}{\mathbb{D}^*\mathbb{D}s} \frac{g^{\uparrow\downarrow}}{4\pi} A^2\kappa^*\kappa \cosh[\kappa^*(d-x)] \cosh[\kappa(d-x)]\right] \\ = \; & (l)^{-2}(t)^{-1} \frac{(E)(t) \times (E)}{(E)^4(l)^4 \times (l)^{-3}} (l)^{-2} \times (E)^2(l)^4 \times (l)^{-2} \\ = \; & \frac{(l)^{-2}(E)^4(t)^0}{(l)^1(E)^4} = (length)^{-3}, \end{aligned}$$

which is what we want, as Aq_y has dimensionality $(energy)(length)$, so that the current has unit $\frac{energy}{(length)^2}$.

F.2 Bulk current

We first compute the dimensionality of $\tilde{\Omega}$:

$$\begin{aligned}[\tilde{\Omega}] &= \left[\int \frac{d^2\mathbf{q}}{(2\pi)^2}\int \frac{d\omega}{2\pi}\frac{-16T}{\omega A\kappa^*\kappa}\frac{1}{\mathbb{D}^*\mathbb{D}}\right] \\ &= (l)^{-2}(t)^{-1}\frac{(E)}{(t)^{-1}\times(E)(l)^2\times(l)^{-2}}\frac{1}{(E)^4(l)^4} = \frac{(l)^{-2}(t)^{-1}(E)^1}{(l)^4(t)^{-1}(E)^5} = \frac{(l)^{-6}}{(E)^4}.\end{aligned}$$

Also, as $[A^2\kappa^*\kappa] = (E)^2(l)^2, \tilde{\beta}_1 = \tilde{\beta}_2 = (E)^2(l)^2$, which leads to the final formula for the bulk current from section 3.4 having dimensionality

$$\begin{aligned}&\left[Aq_y\tilde{\Omega}\tilde{\beta}_1 A^2\kappa^*\kappa\left\{\kappa\left[\sinh[\kappa x]\cosh[\kappa^* x]\right]\right\}\right] \\ &= (E)(l)^2\times(l)^{-1}\times(l)^{-6}(E)^{-4}\times(E)^2(l)^2\times(E)^2(l)^4\times(l)^{-3} = \frac{E}{(l)^2}.\end{aligned}$$

Given that current has unit $\frac{energy}{(length)^2}$, this is what we want.

Appendix G

Computation of the longitudinal current with DMI at $x = d$

G.1 The interfacial longitudinal current at $x = d$

To compute the interfacial longitudinal current at $(x = d)$, we use the formula

$$\left\langle \hat{j}_x^{(I)}(x) \right\rangle_d = A\mathrm{Im}[\langle \psi^* \partial_x \psi \rangle]_d.$$

The motivation for this formula can be found in the beginning of Appendix C. We see. that

$$\left\langle \hat{j}_y^{(I)}(x) \right\rangle_d = A\mathrm{Im}\left[\left\langle (\underbrace{(C_1 e^{\kappa x} + C_2 e^{-\kappa x})}_{\Xi})^* \kappa \underbrace{(C_1 e^{\kappa x} - C_2 e^{-\kappa x})}_{\Gamma} \right\rangle \right]_d .$$

We now calculate this current at $x = d$:

$$\begin{aligned}
\Xi &= C_1 e^{\kappa d} + C_2 e^{-\kappa d} \\
&= (\mathcal{D} e^{-\kappa d} h_L - \mathcal{B} h_R) \frac{e^{\kappa d}}{\mathbb{D}\sqrt{s}} + (-\mathcal{C} e^{\kappa d} h_L + \mathcal{A} h_R) \frac{e^{-\kappa d}}{\mathbb{D}\sqrt{s}} \\
&= \left(\left[A\kappa + i \frac{g^{\uparrow\downarrow}}{4\pi s} \hbar\omega \right] - \left[-A\kappa + i \frac{g^{\uparrow\downarrow}}{4\pi s} \hbar\omega \right] \right) \frac{h_L}{\mathbb{D}\sqrt{s}} \\
&\quad + \left(- \left[-A\kappa + i \frac{g^{\uparrow\downarrow}}{4\pi s} [\hbar\omega - \mu'] \right] e^{\kappa d} + \left[A\kappa + i \frac{g^{\uparrow\downarrow}}{4\pi s} [\hbar\omega - \mu'] \right] e^{-\kappa d} \right) \frac{h_R}{\mathbb{D}\sqrt{s}} \\
&= A\kappa \frac{2h_L}{\mathbb{D}\sqrt{s}} + \left[A\kappa \cosh[\kappa d] - i \frac{g^{\uparrow\downarrow}}{4\pi s} [\hbar\omega - \mu'] \sinh[\kappa d] \right] \frac{2h_R}{\mathbb{D}\sqrt{s}},
\end{aligned}$$

and

$$\begin{aligned}
\Gamma &= C_1 e^{\kappa d} - C_2 e^{-\kappa d} \\
&= (\mathcal{D} e^{-\kappa d} h_L - \mathcal{B} h_R) \frac{e^{\kappa d}}{\mathbb{D}\sqrt{s}} - (-\mathcal{C} e^{\kappa d} h_L + \mathcal{A} h_R) \frac{e^{-\kappa d}}{\mathbb{D}\sqrt{s}} \\
&= \left(\left[A\kappa + i \frac{g^{\uparrow\downarrow}}{4\pi s} \hbar\omega \right] + \left[-A\kappa + i \frac{g^{\uparrow\downarrow}}{4\pi s} \hbar\omega \right] \right) \frac{h_L}{\mathbb{D}\sqrt{s}} \\
&\quad + \left(- \left[-A\kappa + i \frac{g^{\uparrow\downarrow}}{4\pi s} [\hbar\omega - \mu'] \right] e^{\kappa d} - \left[A\kappa + i \frac{g^{\uparrow\downarrow}}{4\pi s} [\hbar\omega - \mu'] \right] e^{-\kappa d} \right) \frac{h_R}{\mathbb{D}\sqrt{s}} \\
&= i \frac{g^{\uparrow\downarrow}}{4\pi s} \hbar\omega \frac{2h_L}{\mathbb{D}\sqrt{s}} \\
&\quad + \left[A\kappa \sinh[\kappa d] - i \frac{g^{\uparrow\downarrow}}{4\pi s} [\hbar\omega - \mu'] \cosh[\kappa d] \right] \frac{2h_R}{\mathbb{D}\sqrt{s}}.
\end{aligned}$$

As $\langle h_L^* h_R \rangle = \langle h_R^* h_L \rangle = 0$, $\langle \psi^* \partial_x \psi \rangle$ equals, using the same shorthand as in section 3.4

$$\begin{aligned}
& \kappa \frac{4 \langle h_L^* h_L \rangle}{\mathbb{D}^* \mathbb{D} s} \quad \xi A \kappa^* \\
+\kappa \frac{4 \langle h_R^* h_R \rangle}{\mathbb{D}^* \mathbb{D} s} \Big\{ & \quad A^2 \kappa^* \kappa \quad \cosh[\kappa^* d] \sinh[\kappa d] \\
& \quad -\chi A \kappa^* \quad \cosh[\kappa^* d] \cosh[\kappa d] \\
& \quad +\chi A \kappa \quad \sinh[\kappa^* d] \sinh[\kappa d] \\
& \quad -\chi^2 \quad \sinh[\kappa^* d] \cosh[\kappa d] \Big\}.
\end{aligned}$$

Using the FDT (Eq. 3.1) leads to

$$\begin{aligned}
\frac{4\kappa}{\mathbb{D}^* \mathbb{D} s} 4 (2\pi)^3 \frac{g^{\uparrow\downarrow}}{4\pi} \hbar T \delta(\mathbf{q} - \mathbf{q}') \delta(\omega - \omega') \Big\{ & \quad \xi A \kappa^* \\
& +A^2 \kappa^* \kappa \quad \cosh[\kappa^* d] \sinh[\kappa d] \\
& -\chi A \kappa^* \quad \cosh[\kappa^* d] \cosh[\kappa d] \\
& +\chi A \kappa \quad \sinh[\kappa^* d] \sinh[\kappa d] \\
& -\chi^2 \quad \sinh[\kappa^* d] \cosh[\kappa d] \Big\},
\end{aligned}$$

so that the current equals

$$A\int\frac{d^2\mathbf{q}}{(2\pi)^2}\int\frac{d\omega}{2\pi}\mathrm{Im}\left[\frac{16\kappa}{\mathbb{D}^*\mathbb{D}s}\frac{g^{\uparrow\downarrow}}{4\pi}\hbar T\left\{\begin{array}{ll}\xi A\kappa^* & \\ +A^2\kappa^*\kappa & \cosh[\kappa^* d]\sinh[\kappa d] \\ -\chi A\kappa^* & \cosh[\kappa^* d]\cosh[\kappa d] \\ +\chi A\kappa & \sinh[\kappa^* d]\sinh[\kappa d] \\ -\chi^2 & \sinh[\kappa^* d]\cosh[\kappa d]\end{array}\right\}\right].$$

G.2 The bulk longitudinal current at $x = d$

We start from the formula

$$\left\langle j_x^{(B)}\right\rangle_d = A\mathrm{Im}[\langle\psi^*(x)\partial_x\psi\rangle]_d,$$

Following the same first steps as in Appendix E, we see that

$$\begin{aligned}\langle\psi^*(x)\partial_x\psi(x)\rangle_d &= \left[\left(\int_0^x dz\int_0^x dy[G^>(x,z)]^*\partial_x G^>(x,y)\frac{s}{A^2}\right.\right.\\ &\left.\left.+\int_x^d dz\int_x^d dy[G^<(x,z)]^*\partial_x G^<(x,y)\frac{s}{A^2}\right)\langle h^*(z)h(y)\rangle\right]_d.\end{aligned}$$

At $x = d$, only the first term is relevant:

$$\langle\psi^*(d)\partial_x\psi(d)\rangle = \left[\int_0^d dz\int_0^d dy[G^>(x,z)]^*\partial_x G^>(x,y)\frac{s}{A^2}\right]_{x=d}.$$

From the boundary condition at $x = d$ (Eq. 3.12), we know

$$\partial_x G^> = i\frac{g^{\uparrow\downarrow}}{4\pi sA}\hbar\omega G^>,$$

so that

$$\begin{aligned}\langle\psi^*(x)\partial_x\psi(x)\rangle_{x=d} &= \left[i\frac{g^{\uparrow\downarrow}}{4\pi sA}\hbar\omega\int_0^x dz\int_0^x dy[G^>(x,z)]^*G^>(x,y)\frac{s}{A^2}\right]_{x=d}\\ &= i\frac{g^{\uparrow\downarrow}}{4\pi sA}\hbar\omega\,\langle\psi^*(x)\partial_x\psi(x)\rangle_{x=d},\end{aligned}$$

so that the longitudinal current equals, using the shorthand $\xi \equiv i\frac{g^{\uparrow\downarrow}}{4\pi s}\hbar\omega$

$$\mathrm{Im}\left[\xi\left\langle\psi^*(x)\partial_x\psi(x)\right\rangle\right]_{x=d}.$$

Comparing this to Eq. E.3 from Appendix E, we see that this expression is the same if we substitute $i\times(Aq_y+\frac{D}{2})$ with ξ and evaluate the expression at $x=d$. Continuing to the final expression of Appendix E, we see that the longitudinal current at $x=d$ equals

$$A\int\frac{d^2\mathbf{q}}{(2\pi)^2}\int\frac{d\omega}{2\pi}\mathrm{Im}\left[\frac{-16T}{\mathbb{D}^*\mathbb{D}}\frac{g^{\uparrow\downarrow}\hbar}{4\pi s}\Bigg(\begin{array}{ll} A^2\kappa^*\kappa & \left\{\kappa\left[\sinh[\kappa x]\cosh[\kappa^* d]\right]\right\} \\ +\chi A\kappa & \left\{\kappa\left[\sinh[\kappa d]\sinh[\kappa^* d]\right]-\kappa^*\left[\cosh[\kappa d]\cosh[\kappa^* d]\right]+\kappa^*\right\} \\ +\chi^2 & \left\{-\kappa\left[\cosh[\kappa d]\sinh[\kappa^* d]\right]\right\}\end{array}\Bigg)\right],$$

where we note that, at $x=d$, $\tilde{\beta}_1$ equals $A^2\kappa^*\kappa$.

G.3 Adding the currents

We take the interfacial current:

$$A\int\frac{d^2\mathbf{q}}{(2\pi)^2}\int\frac{d\omega}{2\pi}\mathrm{Im}\left[\frac{16\kappa}{\mathbb{D}^*\mathbb{D}s}\frac{g^{\uparrow\downarrow}}{4\pi}\hbar T\Bigg\{\begin{array}{ll} \xi A\kappa^* & \\ +A^2\kappa^*\kappa & \cosh[\kappa^* d]\sinh[\kappa d] \\ -\chi A\kappa^* & \cosh[\kappa^* d]\cosh[\kappa d] \\ +\chi A\kappa & \sinh[\kappa^* d]\sinh[\kappa d] \\ -\chi^2 & \sinh[\kappa^* d]\cosh[\kappa d]\end{array}\Bigg\}\right]$$

which equals

$$A\int\frac{d^2\mathbf{q}}{(2\pi)^2}\int\frac{d\omega}{2\pi}\mathrm{Im}\left[16\frac{g^{\uparrow\downarrow}}{4\pi s}\frac{\hbar T}{\mathbb{D}^*\mathbb{D}}\kappa\Bigg\{\begin{array}{ll} \xi A\kappa^* & \\ +A^2\kappa^*\kappa & \cosh[\kappa^* d]\sinh[\kappa d] \\ -\chi A\kappa^* & \cosh[\kappa^* d]\cosh[\kappa d]\end{array}\right.$$

$$
\begin{array}{ll}
+\chi A\kappa & \sinh[\kappa^* d]\sinh[\kappa d] \\
-\chi^2 & \sinh[\kappa^* d]\cosh[\kappa d]
\end{array}
\Big\}\Big],
$$

and compare it to the bulk current:

$$
A\int\frac{d^2\mathbf{q}}{(2\pi)^2}\int\frac{d\omega}{2\pi}\mathrm{Im}\Big[-16\frac{g^{\uparrow\downarrow}}{4\pi s}\frac{\hbar T}{\mathbb{D}^*\mathbb{D}}\kappa\Big(
\begin{array}{ll}
A^2\kappa^*\kappa & \Big\{\Big[\sinh[\kappa x]\cosh[\kappa^* d]\Big]\Big\} \\
+\chi A\kappa & \Big[\sinh[\kappa d]\sinh[\kappa^* d]\Big] \\
-\chi A\kappa^* & \Big[\cosh[\kappa d]\cosh[\kappa^* d]\Big] \\
+\chi A\kappa^* & \\
+\chi^2 & \Big\{-\Big[\cosh[\kappa d]\sinh[\kappa^* d]\Big]\Big\}\Big)\Big].
\end{array}
$$

Adding these together yields

$$
\begin{aligned}
& A\int\frac{d^2\mathbf{q}}{(2\pi)^2}\int\frac{d\omega}{2\pi}\mathrm{Im}\Big[16\frac{g^{\uparrow\downarrow}}{4\pi s}\frac{\hbar T}{\mathbb{D}^*\mathbb{D}}\kappa\Big[\xi A\kappa^*-\chi A\kappa^*\Big]\Big] \\
= \; & A\int\frac{d^2\mathbf{q}}{(2\pi)^2}\int\frac{d\omega}{2\pi}\mathrm{Im}\Big[16i\left(\frac{g^{\uparrow\downarrow}}{4\pi s}\right)^2\frac{\hbar T}{\mathbb{D}^*\mathbb{D}}\kappa\Big[\mu' A\kappa^*\Big]\Big] \\
= \; & A\int\frac{d^2\mathbf{q}}{(2\pi)^2}\int\frac{d\omega}{2\pi}16\left(\frac{g^{\uparrow\downarrow}}{4\pi s}\right)^2\frac{\hbar T}{\mathbb{D}^*\mathbb{D}}A\kappa^*\kappa\mu'.
\end{aligned}
$$